

Surface and Subsurface Reactions of Lithium Transition Metal Oxide Cathode Materials: An Overview of the Fundamental Origins and Remedying Approaches

Biwei Xiao and Xueliang Sun*

Lithium-ion batteries (LIBs) have become one of the most prevailing techniques for rechargeable batteries. Lithium transition metal oxides are prevalent cathode materials currently, but they face great challenges due to unsatisfactory energy density, chemical/electrochemical instability, and elemental scarcity concerns. Surface/subsurface is the interface where lithium ions cross between the electrolyte and the cathode materials. Its properties and complicated nature are unambiguously regarded as a crucial controlling factor for the overall performance. Tremendous efforts have been made in the exploration of surface modification methods with remarkable progress hitherto. The purpose of this work is to review these surface behaviors in order to understand their fundamental origins and provide a summary of various surface modification methods that can be used to address impeding issues. Finally, a rational method of surface modification is proposed for use in cathode materials.

1. Introduction


The aggressive consumption of fossil fuels has resulted in the uncontrolled release of greenhouse gases such as carbon dioxide and methane into the atmosphere, trapping heat and causing havoc to the environment. With this in mind, the development of sustainable energy is imperative. Renewable energy will fail to reach the anticipated impact unless more efficient way to store and use electricity is found. Therefore, high-performance energy-storage devices with high energy and power density are required for renewable energy sustainability and storage security. Electrochemical batteries have been long considered as one of the most qualified candidates for providing reliable energy storage. Taking into account the safety, power density, cost, longevity and efficiency, rechargeable lithium-ion batteries (LIBs) are the most successful electrochemical storage systems available. The extensive

application of LIBs is not limited to the portable electronics market, but is also expediting the paradigm shift in the transportation sector toward the use of electric vehicles. Although hybrid vehicles utilizing LIBs are already commercially available by automotive manufacturers, a great deal of innovation is still required in order to achieve the energy density, safety and cost stated by the United States Advanced Battery Consortium Goals for Advanced Batteries for EVs—CY 2020 Commercialization.^[1,2]

LIBs have attracted massive attention after being commercialized by SONY in 1991 due to their high energy density, good performance and long cycling life compared to conventional Ni–H, Ni–Cd, and Pb–acid batteries.^[3] The growing demand for LIBs during the last

two decades have stimulated enormous investigations on the development of high performance electrode materials. A LIB is typically comprised of three major components, the cathode, anode and electrolyte. Primary prototype LIBs were based on the LiCoO₂/Li system, where LiCoO₂ was the cathode material and lithium metal was the anode material. Charge/discharge cycling was achieved on the basis of lithium intercalation and de-intercalation from the LiCoO₂ layered structure. The metallic lithium was later replaced by carbonaceous materials in secondary LIBs due to safety concerns. In addition to carbonaceous materials, a myriad of other materials were reported to be eligible as potential anode materials, such as Sn, Si, Li₄Ti₅O₁₂, metal oxides, etc.^[4] In sharp contrast to the diversity of anode materials available for use, the number of applicable cathode materials is significantly underdeveloped. Despite the fact that the intercalation chemistry has been comprehensively studied over centuries, the categories of cathode materials are rather scarce.^[5] Primary groups of cathode materials include the layered LiCoO₂, spinel LiMn₂O₄, poly-anion LiFePO₄, and their derivatives. Within these classes of cathode materials, LiFePO₄ was a very hot topic in the late 2000s and early 2010s. In recent years, lithium transition metal oxides became the prevalent research topic because they offer much higher energy density than LiFePO₄. This review paper concentrates on the surface and subsurface issues of lithium transition metal oxides. **Figure 1** shows the cost breakdown of a sample PHEV20 battery pack, materials cost 61% of the pack. Within

Dr. B. Xiao, Prof. X. Sun
Department of Mechanical and Materials Engineering
University of Western Ontario
London, ON N6A 5B9, Canada
E-mail: xsun@eng.uwo.ca

 The ORCID identification number(s) for the author(s) of this article can be found under <https://doi.org/10.1002/aenm.201802057>.

DOI: 10.1002/aenm.201802057

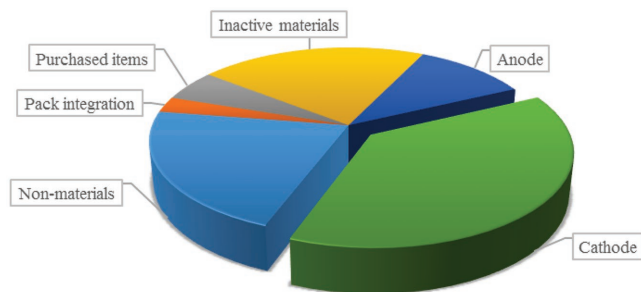


Figure 1. Breakdown of the material cost in a typical PHEV20 battery pack. (Data were adapted from ref. [2]).

the seven major components of the materials, cathode materials cost 38%,^[2,6] the most critical reasons are the difficulty of materials manufacturing and the low abundance of lithium, cobalt, manganese, and nickel that dominate the current LIBs market. As a result, the relatively slow development of cathode materials serves as a major hindrance toward lowering the cost and efficiency of future LIBs.^[7]

In order to maximize the efficiency of a cathode material, researchers have explored the use of advanced materials along with the development of various synthetic methods and modification of existing materials.^[8] While all of these directions have been under rigorous investigation, the topic will always end up with a critical concern—the materials surface. The surface is where lithium ions or electrons diffusion through in the material ends and transfer into the electrolyte or conductive agent, thus the majority of the side reactions happen here due to nonequilibrium diffusion reactions.^[9] Attempts of surface modification aimed at adjusting the chemical or physical properties of the surface have been made within the past decades, but the underlying mechanisms governing these reactions have yet to be completely realized. It is therefore of great importance to review the latest progress, especially in emerging areas such as lithium-rich and Ni-rich cathode material surface modifications and surface modification techniques such as atomic layer deposition (ALD) and molecular layer deposition (MLD). In this work, rather than chronicling experimental results, we present a comprehensive review of surface modification methods on lithium metal oxide cathode materials by starting with an understanding of the fundamental origins of surface behaviors, followed by possible explanations to how surface modification works and a prospect of advanced surface modification methods.

2. Surface Behaviors of Cathode Materials

2.1. Surface Phase Reconstruction

2.1.1. Layered LiMeO_2 ($\text{Me} = \text{Co}, \text{Mn}, \text{Ni}$)

Owing to the considerable voltage, capacity, and easy of scalability, LiCoO_2 has been by far the most successful cathode material for use in LIBs. Layered LiCoO_2 belongs to a rhombohedral space group $R\bar{3}m$ with edge-sharing CoO_6 octahedra, which gives CoO_2 sheets.^[10] Lithium ions reside in octahedral



Biwei Xiao is currently a post-doctoral research associate at Pacific Northwest National Laboratory. He obtained his Ph.D. degree from Prof. Xueliang Sun's group in University of Western Ontario in 2017 and received his Bachelor degree in Materials Science and Engineering from Sichuan University, China in 2011. His research has

been focusing on cathode materials for both lithium-ion batteries and sodium-ion batteries, carbon materials, and synchrotron radiation techniques.



Xueliang Sun is a Canada Research Chair in Development of Nanomaterials for Clean Energy, Fellow of the Royal Society of Canada and Canadian Academy of Engineering and Full Professor at the University of Western Ontario, Canada. He received his Ph.D. in materials chemistry in 1999

from the University of Manchester, UK, which he followed up by working as a postdoctoral fellow at the University of British Columbia, Canada. His current research interests are focused on advanced materials for electrochemical energy storage and conversion, including electrocatalysis in fuel cells and electrodes in lithium based batteries and metal–air batteries.

sites between the CoO_2 sheets so that electrochemical deintercalation forms Li_xCoO_2 .^[11] Despite having a calculated theoretical capacity of 272 mAh g^{-1} , LiCoO_2 can only be deintercalated to $\text{Li}_{0.5}\text{CoO}_2$ within a cutoff voltage of 4.2 V without severe degradation, and reduces the available reversible capacity to half of its theoretical value.^[11] This diminished capacity value stems from LiCoO_2 undergoing a phase transition from a layered structure to a quasi-spinel (QS) one when half of the lithium is deintercalated. It is suggested that the transition is a result of Co migration into Li planes due to elevated thermal diffusivity.^[12] Dahn et al. initially reported the synthesis of QS- LiCoO_2 (or in some cases written as $\text{Li}_{1+y}\text{Co}_2\text{O}_4$) in a space group of $\text{Fd}\bar{3}m$ under low temperature (400 °C), the thermodynamic stability of which is lower than that of layered LiCoO_2 .^[13] Various approaches to synthesizing LiCoO_2 with both layered and quasi-spinel configurations were reviewed by Antonelli.^[14] A comprehensive study of the two phases revealed that the QS- LiCoO_2 possesses much lower capacity and higher polarization compared to layered LiCoO_2 , thus turning out to be an inferior candidate for use in LIBs.^[13] X-ray absorption

near-edge spectra (XANES) confirmed that there are intermediate phases between the layered and spinel structures due to the higher oxidation state of spinel LiCoO_2 ,^[15] it was thereafter found to be $\text{Li}_x\text{Co}_{1-x}[\text{Co}_2]\text{O}_4$ by Thackeray et al.^[16]

The formation of spinel phase in layered LiCoO_2 initiates at the surface and extends to the bulk under severe conditions such as prolonged intensive cycling, operation in an extended voltage window and use under high temperature. Transmission electron microscopy (TEM) studies revealed the formation of dislocations and internal strains within the lattice of LiCoO_2 even at low cycle numbers. The accumulation of these defects was found to be directly responsible for long term capacity fade, which is related to crackings that will be introduced in Section 2.2.^[17] The presence of strains indicates that the interlayer spacing within LiCoO_2 lattice has been altered, which is in accordance with the in situ X-ray diffraction (XRD) studies carried out by Dahn et al.^[12] A later study found

that post-thermal treatment of LiCoO_2 forms a thin spinel $\text{Li}_x\text{Co}_2\text{O}_4$ film on the surface and improves the performance significantly due to the conductive nature of the spinel phase.^[18] This report is however in contradiction to previous studies, probably due to the different formation mechanisms of this phase.

The phase transformation of a layered structure to a spinel one has also been observed in other metal oxide cathodes such as LiNiO_2 and LiMnO_2 , which are analogous to layered LiCoO_2 as shown in Figure 2a.^[19,20] Each of these ending members of LiMeO_2 (Me = Ni, Co, Mn) possesses its unique advantages as a cathode material. Nevertheless, apart from structural transitions, these materials suffer from severe Jahn-Teller distortion, which is another major contributing factor toward capacity decay.^[21,22] In the case of LiNiO_2 , the low spin Ni^{3+} ion has a $t_{2g}^6 e_g^1$ 3d electronic configuration. The Jahn-Teller distortion can be induced by the e_g energy level, which results in

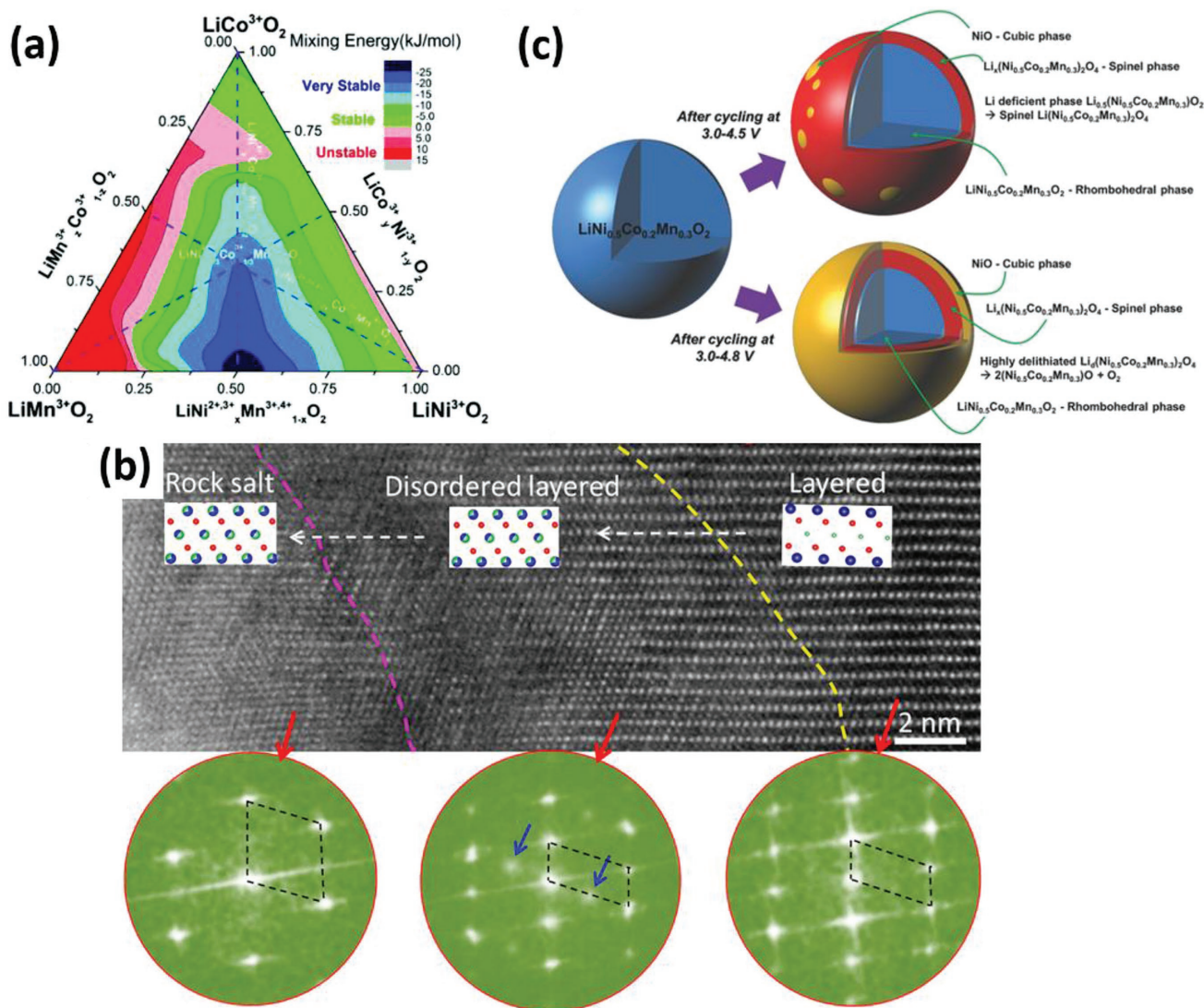


Figure 2. a) Compositional phase diagram of LiMnO_2 - LiNiO_2 - LiCoO_2 . Reproduced with permission.^[20] Copyright 2017, Royal Society of Chemistry. b) Reconstructed surface layer of NMC333 after 100 cycles within 2.0–4.8 V. Reproduced with permission.^[27] Copyright 2017, American Chemical Society 2017. c) Degradation mechanism of Ni-rich $\text{LiNi}_{0.5}\text{Co}_{0.2}\text{Mn}_{0.3}\text{O}_2$. Reproduced with permission.^[28] Copyright 2014, Wiley-VCH.

the disproportionation reaction of Ni^{3+} and the formation Ni^{2+} and Ni^{4+} that have two e_g electrons and no e_g electron respectively.^[22] Initial observation of the Jahn-Teller distortion occurring in LiNiO_2 was reported by Delmas et al. in 1995.^[21] Through the application of extended X-ray absorption fine structure (EXAFS) studies, two Ni–O bond lengths with 1.91 and 2.09 Å were found to exist in LiNiO_2 . Unlike Ni^{3+} , the 3d electronic configuration of Co^{3+} is $t_{2g}^6 e_g^0$, with one less e_g electron, therefore, the Jahn-Teller distortion in LiCoO_2 is absent.^[22] As a result, plenty of effort has been dedicated to the investigation of dopants induced suppression, such as the inclusion of Al, Co, Mn, Cr, etc.^[23] The fundamental principle behind this is to lower the concentration of the Jahn-Teller effective ions. For instance, doping LiNiO_2 with Co to form $\text{LiCo}_{0.5}\text{Ni}_{0.5}\text{O}_2$ has been suggested to change the Ni electronic configuration from $t_{2g}^6 e_g^1$ to $t_{2g}^6 e_g^2$, which is Jahn-Teller inactive.^[24]

Attempts toward doping layered metal oxides introduced numerous derivatives, which are of remarkable value now. Among them, $\text{LiNi}_x\text{Mn}_y\text{Co}_{1-x-y}\text{O}_2$ (NMC) and $\text{LiNi}_{0.8}\text{Co}_{0.15}\text{Al}_{0.05}\text{O}_2$ (NCA) have found applications in current electrical vehicles. The high operational voltage and specific capacity have made these materials outperform many other cathode materials.^[25,26]

Within the category of NMC layered cathode materials, $\text{LiNi}_{1/3}\text{Mn}_{1/3}\text{Co}_{1/3}\text{O}_2$ with a ratio of 1:1:1 (NMC111) has been intensively studied since it combines the rate performance of LiCoO_2 , safety of LiMnO_2 and capacity of LiNiO_2 . The surface reconstruction upon aggressive exposure to electrolyte has, however, also been reported in these materials, as shown in Figure 2b.^[26,27] In an attempt to achieve high energy density cathode materials for EVs, Ni-rich NMC with high capacity has become a focus in recent years. The rich Ni content in the material, however, involves safety issues, preparation difficulty and storage concerns.^[28,29] Due to the similar ionic radii and

oxidation state with Li^+ , Ni^{2+} in Ni-rich NMC materials has been found to show very high degree of interlayer mixing between these two elements, resulting in strong phase segregation and capacity fade.^[30] Figure 2c shows a schematic illustration of the degradation mechanism of a Ni-rich $\text{LiNi}_{0.5}\text{Co}_{0.2}\text{Mn}_{0.3}\text{O}_2$ (NMC523) material. In this study, different degradation mechanisms from NMC111 are proposed, specifically, the O3 to O1 phase transformation at highly delithiated conditions, which involves the gliding of the TMO_2 layers. This mechanism was found to be a primary reason for rapid capacity fade in NMC523 due to the formation of stacking fault. However, no such phase transformation was observed in NMC111, probably due to the lower Ni–Li site exchange. These studies have unambiguously demonstrated that stabilization of Ni in Ni-rich NMC cathodes is imperative to enable stable and reliable energy storage performance. A possible strategy is to design a Ni rich bulk and Mn rich surface NMC material. This concentration gradient has been proven to be effective in controlling the surface Ni disorder.^[31,32] An extreme case reported recently synthesized a core-shell structure with LiNiO_2 as the core encapsulated by a $\text{LiNi}_{0.87}\text{Co}_{0.065}\text{Mn}_{0.065}\text{O}_2$ shell, which achieved a capacity of more than 230 mAh g^{-1} and 74.2% capacity retention after 100 cycles.^[33]

2.1.2. Layered Lithium-Rich Oxides

Layered Li-rich NMC can be written as $x\text{Li}_2\text{MnO}_3 \cdot (1-x)\text{LiMeO}_2$ (Me = Ni, Co, Mn), it is regarded as the combination of a LiMeO_2 phase (trigonal, $R\bar{3}m$) and a Li_2MnO_3 phase (monoclinic, $C2/m$) as shown in Figure 3a.^[34] Compared to conventional layered LiMeO_2 , the Li_2MnO_3 material has lithium ions occupying part of the transition metals in the transition metal layer and they form LiMn_6 units, therefore the Li_2MnO_3 phase

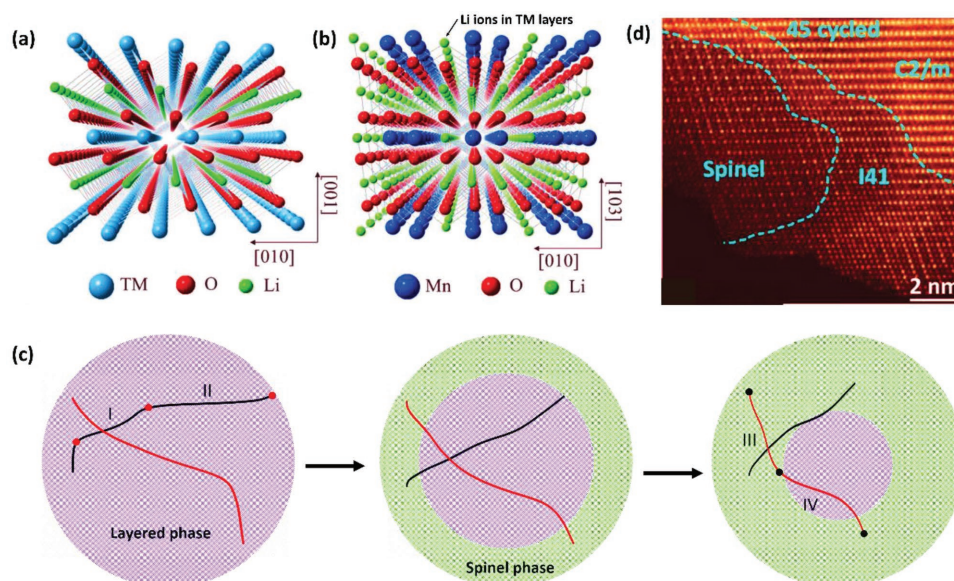
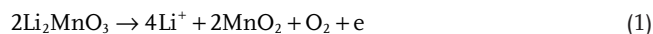


Figure 3. Structures of a) layered trigonal LiMeO_2 and b) layered monoclinic Li_2MnO_3 viewed from the [100] crystallographic direction. Adapted with permission.^[36] Copyright 2013, Wiley-VCH. c) Schematic diagram showing the charge/discharge curves of a typical Li-rich NMC with the evolution of structure during cycling. d) STEM-HAADF image of a cycled Li-rich $\text{Li}_{1.2}\text{Ni}_{0.2}\text{Mn}_{0.6}\text{O}_2$ showing the presence of a spinel phase on the surface. Adapted with permission.^[37] Copyright 2015, American Chemical Society.

can be also reformulated as $\text{Li}[\text{Li}_{1/3}\text{Mn}_{2/3}]\text{O}_2$, where 1/3 of the Mn sites are occupied by lithium ions.^[35]

Though the fact that the structure of Li-rich NMC material is formed by the combination of LiMeO_2 and Li_2MnO_3 is clear, the mixing of these two phases has recently been intensively contested. The main argument is whether the final structure is a solid-solution as a result of Li_2MnO_3 integrated into the trigonal structure of LiMeO_2 or the formation of nanodomains of these two phases and Li_2MnO_3 helps stabilize the structure of LiMeO_2 . Ikuhara et al.^[36] used electron diffraction and annular bright field (ABF) scanning transmission electron microscopy (STEM) combined with high-angle annular dark-field (HAADF) STEM techniques to investigate the phase components of Li-rich NMC material synthesized via a solid-state reaction method. They found that two phases that can be ascribed to rhombohedral (rh) LiMeO_2 and monoclinic (mon) Li_2MnO_3 -like structure coexist in the observed domain. The two phases were found to have been separated by the (001)rh/(103)mon plane, revealing that they presented independently as nanodomains in the Li-rich NMC material. On the other hand, many other researchers have unambiguously found that these two phases form solid solutions by telling that the material is made up of a single phase.^[38,39] The reason why different researchers have obtained strikingly different results may be ascribed to the fact that the materials they studied were not synthesized from the same method and that the composition was not essentially the same, where transition metal ratios vary.^[39]

The high capacity of Li-rich NMC derives from its unique structure. In the Li-rich NMC with a composition of $x\text{Li}_2\text{MnO}_3 \cdot (1-x)\text{LiMeO}_2$ (Me = Ni, Co, Mn), conventional LiMeO_2 and Li_2MnO_3 are activated individually. As shown in Figure 3c, in region I, delithiation occurs within the LiMeO_2 phase, alongside the oxidation of Co and Ni. The subsequent long plateau marked as II corresponds to the activation of the Li_2MnO_3 , the reaction can be summarized as follows



The oxygen release in the first charge process, together with the removal of lithium ions in the transition metal layer, yield a net loss of Li_2O and the formation of layered MnO_2 . In the following discharge process, the following reaction occurs



Clearly, compared to conventional LiMeO_2 , an extra reversible lithium insertion into layered MnO_2 has taken place in the Li-rich NMC materials, which allows for a discharge capacity of over 250 mAh g^{-1} .^[40] The concomitant removal of oxygen and lithium ions from the Li_2MnO_3 leaves lithium vacancies in the transition metal layer with O vacancies occurring at the octahedral edges. This structure is inherently unstable and results in the adjacent transition metals, especially Ni, to drop into Li vacancies in the Li layer.^[41] The mechanism is similar with the aggregation of spinel phase in conventional layered NMC materials surfaces. Nevertheless, in the case of Li-rich NMC, this reaction is more intense due to the higher instability of the transition metals. The consequence of the growth of spinel phase can be found in Figure 3c as well. Region III represents the

capacity delivered from a layered phase and region IV stands for the spinel phase. It can be seen that upon extended cycling, more of the capacity stems from region IV, indicating that the spinel phase gradually grows and the layered phase diminishes. A STEM-HAADF image of a cycled Li-rich NMC clearly shows spinel phase on the surface, as shown in Figure 3d. The average voltage of the spinel phase is normally only 2.8 V, which is much lower than the layered phase, therefore the mean voltage of the whole cell drops.^[42] On the other hand, the spinel phase consists of Mn in a lower valence state, it is known that Mn^{3+} undergoes Jahn-Teller distortion and forms Mn^{2+} and Mn^{4+} . Furthermore, Mn^{2+} is soluble in the electrolyte, resulting in loss of active material and rapid capacity fading. In summary, structural transformations in Li-rich NMC is detrimental to its Li storage performance and, finding a method to stabilize the surface of the material is of paramount importance. A recent study investigated the spinel phase formation on Li-rich NMC particles with various morphologies and found that it is indeed facet-dependent, with the least formation in the direction where transition metal layer stacks.^[43]

Oxygen participation in the charge compensation process is another problem that plagues this material. The higher than expected capacity of Li-rich NMC has lead thorough investigation pertaining to the behavior of oxygen during electrochemical cycling. In situ XAS was employed to systematically track the valence and bond length changes of transition metals within the material during electrochemical cycling. It was found that the valence change during the initial discharge process was not able to account for the high discharge capacity.^[44] Furthermore, the electrolyte decomposition product with the presence of oxygen is different from regular cases. The oxygen anion redox charge compensation tends to result in more Li_2CO_3 formation.^[45]

2.1.3. Spinel LiMn_2O_4

Spinel type LiMn_2O_4 belongs to the space group symmetry of $\bar{3}m$, in which Mn shows an average valence of 3.5, indicating the coexistence of Mn^{3+} and Mn^{4+} .^[46] However, the equilibrium can be easily broken by Li^+ insertion or temperature change, causing Jahn-Teller distortion of Mn^{3+} at the octahedral sites. The onset of Jahn-Teller distortion at 4.0 V has been regarded as a primary source of capacity loss.^[47] Studies conducted on the surface structure of LiMn_2O_4 revealed that a net valence difference is present between the surface and bulk, with more Mn^{3+} present on the surface due to the nonequipoised dynamic of Li^+ insertion (C-rate controlled) and extraction (diffusion-controlled).^[48,49] This was suggested to result in the formation of $\text{Li}_2\text{Mn}_2\text{O}_4$, which is much less electrochemically reactive.^[50] Nonetheless, the phase transition from cubic to tetragonal, induced by the Mn^{3+} Jahn-Teller distortion, was speculated to generate a phase boundary on the particle surfaces and severely limits lithium-ion diffusion. Similar to strategies involving the doping of elements in layered LiMeO_2 , doping of LiMn_2O_4 has also been a vastly studied topic aimed at suppressing the Jahn-Teller distortion.^[46,49] Of various possible doping elements, Ni has been employed to form $\text{P4}_32 \text{LiNi}_{0.5}\text{Mn}_{1.5}\text{O}_4$ and was found to be successful due to the electrochemical reactivity of

Ni^{2+} and the disappearance of Mn^{3+} .^[51] Furthermore, the incorporation of Ni^{2+} provides two voltage plateaus at about 4.7 V ($\text{Ni}^{2+}/\text{Ni}^{3+}$, $\text{Ni}^{3+}/\text{Ni}^{4+}$), making it a very promising high power cathode material. Although trace amount of Mn^{3+} was reported in oxygen-deficient $\text{LiNi}_{0.5}\text{Mn}_{1.5}\text{O}_{4-\delta}$ with a space group $\text{Fd}\bar{3}m$, the Jahn-Teller distortion is significantly suppressed.^[52]

2.2. Stress-Induced Cracking

Mechanical cracking has been primarily reported for anode materials that undergo large volume expansion upon lithiation, such as Si and Sn. Cathode materials, however, have also been found to develop cracks upon high rate cycling when the lithium ions do not have sufficient time to diffuse homogeneously, ending up with extra stress in particles.^[53] For a brittle cathode material, the C-rate that is required to initiate cracks decreases with increasing particle size.^[54] The residual internal stress of electrode materials during preparation and phase change (such as Jahn-Teller distortion, O_2 release) induced stress can also aid in the development of cracks in the materials surface and eventually propagate to the bulk.^[55,56] In a broader scope, cracks can be defined as both intergranular crack and intergranular crack depending on the cracking locations. **Figure 4a–f** shows a typical intragranular crack lattice. The crack was developed from dislocations that are universal in as-prepared materials, upon cycling, the TMO_2 layers became loosely connected due to the propagation of the dislocations, resulting in a wider interslab distance, which will eventually turn into a macroscopic crack.^[56] A recent study has revealed that the thermal stress and pressure increase generated during the battery operation can lead to very strong phase inhomogeneity, which is also a direct reason for the abrupt intragranular cracks development.^[56,57] On the other hand, if the volume change of the cathode materials is nonelastic deformation, it will lose contact with the binders and conductive carbon, forming intergranular cracks. The occurrence of intergranular cracks segregates part of the materials from the electrolyte and leads to the increase of impedance and subsequent battery failure. In situ SEM studies conducted on $\text{LiNi}_{0.8}\text{Co}_{0.15}\text{Al}_{0.05}\text{O}_2$ shows direct visual evidence of cracks developing and separating the active materials from the electrolyte, as shown in **Figure 4g,h**. Surprisingly, the development of cracks was found to occur in the first cycle, indicating the necessity to develop strategies that can prevent the cracking of cathode materials. A schematic diagram showing the consequence of the cracking toward lithium diffusion is presented in **Figure 4i**. Zhang et al. investigated the formation of cracks in on lithium rich layered $\text{Li}[\text{Li}_{0.2}\text{Ni}_{0.2}\text{Mn}_{0.6}]\text{O}_2$.^[58] Following long term cycling, microcracks were found in the particles due to the large stress caused by simultaneous removal of lithium and oxygen, resulting in pulverized surface structures. Mn ions on the surface were found to be reduced, as revealed by electron energy loss spectroscopy (EELS), indicating an inhomogeneous surface chemistry.

In addition to the cracking at the materials level, there is also cracking problems when it comes to thick electrode with high mass loading. The thick electrode results in heterogeneous state of charge (SOC) from the surface to the bulk, leading to polarization of the cell and delamination from the current collectors.^[59]

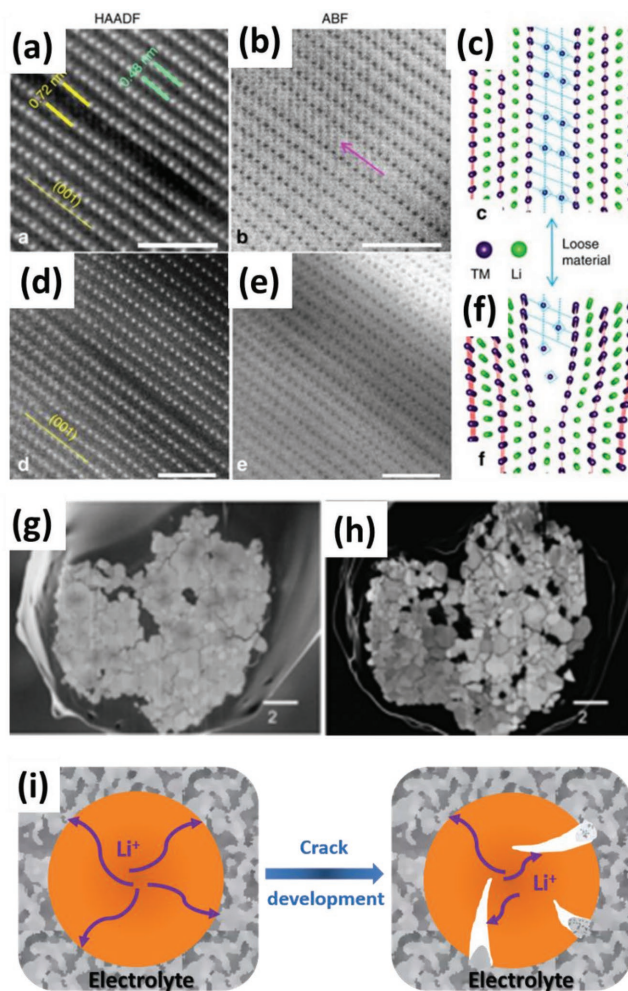


Figure 4. a,b) HAADF and ABF images showing a loose lattice in cycled $\text{LiNi}_{1/3}\text{Co}_{1/3}\text{Mn}_{1/3}\text{O}_2$ along the [010] axis; c) the corresponding lattice model. d,e) HAADF and ABF images showing a crack tip; f) the corresponding lattice model. Reproduced with permission.^[56] Copyright 2017, Springer Nature. SEM images of $\text{LiNi}_{0.8}\text{Co}_{0.15}\text{Al}_{0.05}\text{O}_2$ particle intergranular cracking after g) 1, h) 4 electrochemical cycles. Reproduced with permission.^[60] Copyright 2013, Wiley-VCH. i) Schematic illustration of the segregation consequences of cracks toward the lithium-ion diffusion.

2.3. Electrolyte Decomposition and Transition Metal Dissolution

2.3.1. Electrolyte Decomposition

Electrolytes for LIBs are generally liquid or solid with electrical conductivity below $10^{-10} \text{ S cm}^{-1}$ and lithium-ion conductivity above $10^{-4} \text{ S cm}^{-1}$.^[1c] In conventional nonaqueous electrolyte, organic carbonate esters based blends, including ethylene carbonate (EC), diethylene carbonate (DEC), propylene carbonate (PC), dimethylene carbonate (DMC) and ethylmethyl carbonate (EMC) are widely used as electrolyte solvents,^[61] with the employment of LiPF_6 salt.^[62] The operational voltage windows of these solvents are typically between 1.0 V and 4.7 V versus Li/Li^+ ,^[63] therefore any cathode materials that require a voltage cutoff value above 4.7 V (in practical 4.5 V due to the catalytic effect of cathode materials) inevitably involve decomposition of

electrolyte via oxidation reaction. The consequence of electrolyte decomposition is the formation of a passivating cathode electrolyte interphase (CEI) layer, comprised of inorganic salts such as Li_2CO_3 , LiF , and organic species such as poly(ethylene carbonate).^[64–66] Recent progress of lithium metal batteries has extended the concentration of the electrolyte to close to the saturation point using lithium bis(fluorosulfonyl)imide (LiFSI) as the salt and bis(fluorosulfonyl)imide (BTfE) as the cosolvent to produce a localized high concentration electrolyte.^[67] However, the decomposition mechanism on the cathode side is not yet fully investigated. The CEI layer is normally electrically insulating yet lithium conductive.^[68] A great deal of research effort has been dedicated toward expanding the electrolyte redox window.^[69] The CEI formation causes irreversible lithium/capacity loss during the first several cycles, in this sense, it is unfavorable to the battery performance.

The intricacy of CEI growth is far from being resolved thus far.^[65] Despite the capacity consumption during the electrolyte decomposition, the oxidation of electrolyte on the surface of cathode materials requires continuous electron transfer,^[1c,70] the electrically insulating layer can keep the electrolyte from being further oxidized, a CEI layer with certain thickness and good stability is therefore desired.^[61,71] In order to mitigate electrolyte decomposition, sacrificial electrolyte additives have been employed.^[72]

Even though CEI formation is a side reaction pertinent to the electrolyte side, heterogeneous and thick CEI has been found to facilitate the degradation of the cathode material structure as well. First, nonuniform coverage of the cathode may lead to leaching of the transition metals out of the structure (see Section 2.3.2 for details). Second, it has been found that thick CEI accelerates the surface phase change due to an uneven lithium diffusion rate on the surface. Third, a thick and nonuniform CEI affect the local delithiation and lithiation levels after prolonged cycling, leading to nonuniform contraction and expansion of the lattice, which eventually turns into intragranular cracks.^[73]

2.3.2. Transition Metal Dissolution

Decomposition of the electrolyte is not the only issues that plague this vital component of LIBs. Although electrolytes are supposed to be nonaqueous, traces amounts of moisture in the electrolyte or on the surface of cathode materials is commonly found. As a result, the LiPF_6 salt may undergo the following dissociation reaction: $\text{LiPF}_6 \rightleftharpoons \text{LiF} + \text{PF}_5$, followed by the hydrolysis of PF_5 : $\text{PF}_5 + \text{H}_2\text{O} \rightarrow \text{POF}_3 + 2\text{HF}$ according to Aurbach and Heider's theory.^[74] Production of HF from the hydrolysis of PF_5 , along with the inherent HF in the LiPF_6 salt, triggers obscure side reactions on the cathode materials.^[61,75] Studies have shown that the dissolution level follows a trend with $\text{Mn} > \text{Co} > \text{Ni}$.^[76]

Taking spinel LiMn_2O_4 as an example, it was found that cathode materials containing more Mn^{3+} tend to suffer from higher manganese dissolution into the electrolyte.^[77] The Mn^{3+} tends to undergo a disproportionation reaction: $2\text{Mn}^{3+} \rightarrow \text{Mn}^{2+} + \text{Mn}^{4+}$, where the Mn^{4+} remains on the material surface and Mn^{2+} dissolves into the electrolyte. Aoshima and colleagues studied the

mechanism of capacity fading in manganese spinels and concluded that the dissolved Mn^{2+} preferentially forms a layer of MnF_2 and ramsdellite- $\text{Li}_{0.5}\text{MnO}_2$ on the surface of the cathode, along with a layer of deposited metal Mn on the anode. These two synergistic processes were responsible for the fade in capacity for manganese spinels.^[50,78–80] A more recent study by Kanno and coworkers found that the Mn dissolution is dependent on which crystal plane is exposed to the electrolyte, with (110) plane being less thermodynamically stable than the (111) plane.^[81] The dissolution of Mn is, however, more intense in cathode materials that operate at higher voltage such as $\text{LiNi}_{0.5}\text{Mn}_{1.5}\text{O}_4$ and under elevated operation temperatures.^[82] The side effect of Mn dissolution, aside from the loss of active materials, also involves degradation of the anode. An “ion-exchange model” was proposed to explain the reaction of Mn on the anode surface.^[79] In detail, Mn^{2+} dissolved into the electrolyte is thought to react with the solid electrolyte interphase (SEI) by undergoing an exchange reaction with the Li^+ . This results in the anode SEI to become Mn-rich while simultaneously hindering lithium diffusion channels, thereby increasing the impedance.

Although Mn dissolution is prevalent among these transition metals, it is necessary to overview the dissolution behaviors of Co and Ni as well. The dissolution of Co is believed to be related to the phase transition at high voltage, as the Co diffuse to Li sites and eventually leach out from the parent structure.^[66] This process can also be accelerated by the generation of HF at such a high voltage. Ni, however, has been found to be more stable than Mn and Co. It is believed that the suppressed Ni dissolution could be related to the stable NiO-like rock salt phase formed on the surface due to phase transition.^[80] In addition, Al-containing Ni-rich $\text{LiNi}_{0.8}\text{Co}_{0.15}\text{Al}_{0.05}\text{O}_2$ material was substantially more stable than Mn-containing Ni-rich $\text{LiNi}_{0.7}\text{Co}_{0.15}\text{Mn}_{0.15}\text{O}_2$ materials, this is partially because that when Mn dissolves, the surface structure destabilizes and leads to the instability of Ni.^[83]

2.4. Surface Instability in Air and Moisture

Storage of Ni-rich and Li-rich NMC materials has been a hassle practically. When exposed to humid air, the Ni^{3+} in these materials spontaneously get reduced to Ni^{2+} , accompanied by the loss of lithium, which accumulates on the material surface in the form of Li_2CO_3 and LiOH through reaction with CO_2 and water.^[84] These impurities deteriorate the performance of the cathode material from several aspects. First, the surface of the cathode materials becomes basic with a PH close to 11, which is detrimental for the slurry preparation process since the binder PVDF undergoes a defluorination process under basic environment,^[85] this leads to further accumulation of impurities on the material surface and the loss of binding functionality, the slurry becomes gel like and is difficult for uniform casting. Second, it has been found that impurities such as Li_2CO_3 decompose under high voltage, generating gas such as CO_2 and CO , which is detrimental for practical batteries.^[86] They also react with the LiPF_6 and consume the available electrolyte.^[87] Third, the loss of lithium on the surface induces irreversible phase transitions, which may block the channels for lithium-ion diffusion.^[88]

3. Roles of Surface Modifications

3.1. Surface Modification as Phase Transition Inhibitor

3.1.1. Surface Structural Design

Bulk doping of cathode materials has been extensively studied over the past few decades. The aim of this process is to control the phase change or enhance the diffusion rate within a particle. However, bulk doping elements, usually Ti, Al and so on, are normally electrochemically inactive. In regard of this, restricting the doping to the material surface has therefore become a prevalent topic since minimum capacity sacrifice is expected in this scenario. Cho et al conducted a number of detailed studies pertaining to the surface protection of LiCoO₂. The majority of their work concluded that metal ions in the coating materials, such as Al, Zr, and Sn were found to migrate into the near surface lattice of the cathode material, forming a solid solution.^[89] His early work in 2000 demonstrated that when the surface of LiCoO₂ was slightly doped with Al, the *c* axis would have 1.7% shift during the first cycle whereas the ones with solid solution on the surface showed only 0.14%, which was also observed in their later report on Zr doped surface. This opinion was however opposed by Dahn et al. They conducted a ZrO₂ coating study on LiCoO₂ with careful examination on the structural change, no difference was observed on the coated and bare samples.^[90,91] Therefore, closer investigation on the mechanism through which surface doping works to suppress phase reconstruction is needed. Park et al. reported an alternative explanation by depositing inhomogeneous MgO onto the surface of LiCoO₂ followed by heat treatment under different temperatures.^[92] Prior to electrochemical cycling, the near surface and bulk structures were identical. However, following electrochemical cycling, additional selected area

diffraction points can be observed on the noncoated areas and the bulk. These weak reflections were proposed to stem from lithium and vacancy ordering and were not observed in coated regions of the sample. Therefore, they concluded that incorporation of Mg into the LiCoO₂ actually occupied Li sites rather than Co sites, resulting in an inhibition of phase transition. Similarly, Cho also reported another possible design for surface solid solution reactions through the use of Ni²⁺ ions to residing within Li slabs near the surface of LiNi_{0.62}Co_{0.14}Mn_{0.24}O₂, with a thickness of about 10 nm. This material showed exceptional structural stability, especially at elevated temperatures.^[93] A later study by Cabana and coworkers adopted Al₂O₃ to modify the surface of LiMn₂O₄ nanoparticles. The researchers observed an epitaxially grown Mn³⁺-depleted phase on the surface of the active material. The replacement of Mn³⁺ by nonsoluble Al³⁺ on the surface reduced the risk of surface destruction and resulted in significant performance enhancement. Dahn et al. estimated the diffusion of Al and Mg into LiCoO₂ upon sintering by Fick's Law and concluded that the interdiffusion distance of Al and Mg with Co increases with the heating temperature. Arrhenius equation was used to calculate the activation energy barrier, the Al³⁺/Co³⁺ couple was found to be 88 kJ mol⁻¹ and the Mg²⁺/Co³⁺ couple was 100 kJ mol⁻¹.^[94] A similar study has also been reported by Amine and co-workers.^[95] Recent work by our group utilizing the combination of atomic layer deposited TiO₂ coating and postannealing process on spinel LNMO revealed that the titanium ions partially diffuse into the tetrahedral sites that were previously occupied by lithium ions, resulting in the formation of a epitaxially grown TiMn₂O₄-like structure, as can be seen from **Figure 5**. It was found that with a properly adjusted thickness of TiO₂ coating followed by annealing, the capacity and stability can be significantly improved, which was ascribed to the suppression of the migration of transition metals into the empty 16c octahedral sites that is essential for lithium-ion diffusion.^[96]

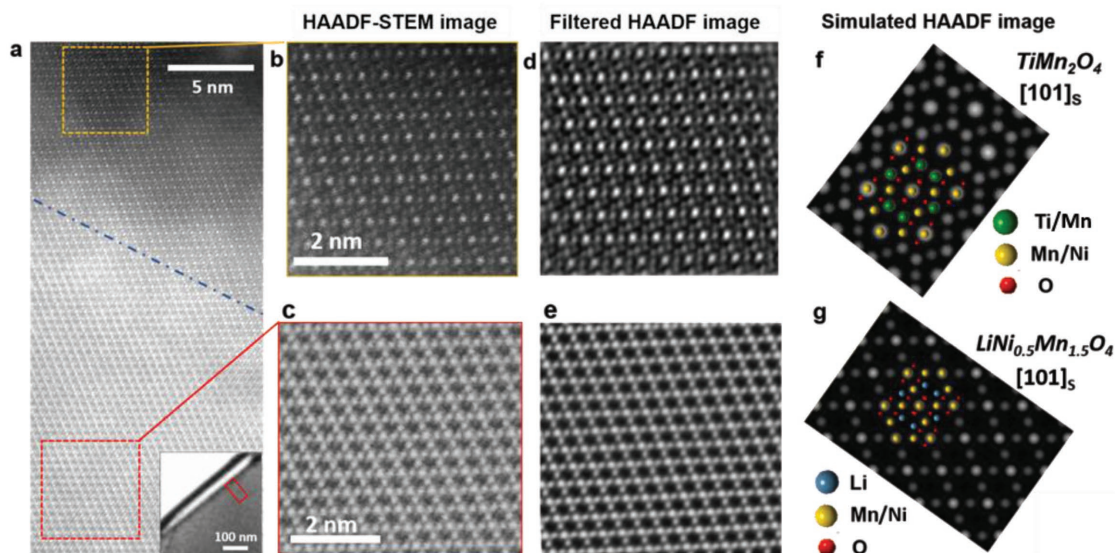


Figure 5. a) HAADF-STEM image of LNMO/250TiO₂A particle acquired near the surface, the corresponding region is shown in the inset image. b,c) Atomic-resolution HAADF-STEM images showing the lattice structure of the outermost layer and the inner region of the particle, respectively. d,e) Processed images corresponding to the HAADF-STEM images shown in (b) and (c) with a band-pass filter applied. f,g) Simulated HAADF images of LiMn₂O₄ and TiMn₂O₄. Reproduced with permission.^[96] Copyright 2017, Wiley-VCH.

The use of surface doping has also resulted in the reduction of Jahn-Teller distortion-caused phase transitions. Taking LiMn_2O_4 as an example, as has been discussed above, the Jahn-Teller distortion predominantly occur at the material surface where the charge equilibrium is broken by lithium diffusion. With respect to this, many researchers believe that modifying only the surface of LiMn_2O_4 , to replace part of the Jahn-Teller active ions, can alleviate performance fade at lowest expense of capacity loss.^[97] Chung et al. adopted a coating material composed of $\text{LiM}_{0.05}\text{Mn}_{1.95}\text{O}_4$ ($M = \text{Co}, \text{Ni}$) to deposit onto the surface of LiMn_2O_4 .^[98] The slightly doped $\text{LiM}_{0.05}\text{Mn}_{1.95}\text{O}_4$ was anticipated to suppress the Jahn-Teller distortions. Similar speculation was also proposed by Xiong et al.^[99] They found that when Al_2O_3 coated LiMn_2O_4 was subject to annealing, the Al that diffused into the surface lattice will help suppress the Jahn-Teller distortion and the remaining crystalline Al_2O_3 shielded the electrolyte from attacking the Mn.

Surface doping has also been shown to be an effective strategy in suppressing the evolution of gaseous O_2 in lithium-rich cathode materials. Previous discussion has implied that the release of O_2 resulted from simultaneous leaching of Li_2O from the layer of Li_2MnO_3 . When hetero atoms are introduced to the surface layers, imported ions may impose extra stress to the Li_2MnO_3 and change its behavior under cycling. This speculation was placed under investigation by Park et al.^[100] in their attempt to improve the performance of a lithium-rich $\text{Li}[\text{Li}_{0.167}\text{Ni}_{0.233}\text{Co}_{0.100}\text{Mn}_{0.467}\text{Mo}_{0.0333}]\text{O}_2$. With the expectation of Al diffusing into the surface lattice, a layer of Al_2O_3 or AlPO_4 was deposited onto the particle surface followed by heat treatment under 600°C for 3 h, the Al was found to have diffused into the surface lattice. By applying a pressure sensor in the battery, they found that when the surface was modified, the pressure dropped noticeably, which is due to the suppressed O_2 release. The basic reason was that the Al incorporated into the surface bonds strongly with the O and simultaneously creates smaller domains of LiMn_2O_3 .

A “pillar effect” was proposed by Cho et al.^[101] The researchers found that by annealing $\text{Mg}_2(\text{PO}_4)_3$ coated $\text{Li}_{1.17}\text{Ni}_{0.17}\text{Co}_{0.17}\text{Mn}_{0.5}\text{O}_2$, Mg can be introduced into the Li (4 h) site. The replacement of Li by Mg was responsible for suppressing voltage fade due to its ability to hinder the migration of transition metals into the Li slab. In this case, the electrochemically inactive Mg act as the pillars. Similarly, Na has been studied as a doping element, as Na ions enlarged the Li^+ slab and helped realize the pinning effect with stabilized structure and faster Li^+ diffusion rate.^[102]

Previous strategies involving solid doping design were almost exclusively focused on diffusing metal ions into the bulk. However, another possible consequence may also occur during this process such as the diffusion of lithium-ions into the coating layer to form a second phase, as proposed by Wu et al.^[103] When a layer of electrochemically active MnO_x was applied to the surface of $\text{Li}[\text{Ni}_{0.2}\text{Li}_{0.2}\text{Mn}_{0.6}]\text{O}_2$ and subject to post annealing, improved performance was reported and was associated with the occurrence of lithium vacancies on the surface diffusion into the MnO_x . The partially lithium-depleted surface resulted in oxygen depleted region, and therefore decreased the chance of O_2 formation. In addition, the MnO_x layer provides additional lithium diffusion channels.^[104] Croy et al. carried out a

delicate study using X-ray absorption spectroscopy (XAS) at the metal K-edges.^[105] They used a Li-Ni-PO_4 composition along with annealing to modify the surface of $\text{Li}_{1.2}\text{Mn}_{0.4}\text{Co}_{0.4}\text{O}_2$ and found that the Ni was not contained within the phosphate and was instead replaced by Li to form a NiMn_6 unit that made the Li_2MnO_3 phase more stable.^[106]

Other methods for surface modification involving treating lithium-rich material with mild acid and hydrazine to partially replace the surface Li^+ with H^+ or incorporate N into the surface.^[107] In a typical example, Meng et al. designed a gas–solid interfacial reaction modification (GSIR) method on Li-rich NMC materials as shown in Figure 6.^[108] The modification was carried out by mixing Li-rich NMC powder with NH_4HCO_3 and heat in an oven placed in the glove box. The decomposition of NH_4HCO_3 under high temperature generates CO_2 gas, which reacts with the surface of the Li-rich NMC powder and creates oxygen vacancies with a depth of 20 nm. Such a treatment was found to boost the performance of the Li-rich NMC material as shown in Figure 6b,c. DEMS study revealed that the O_2 and CO_2 gas release was suppressed in the GSIR-treated sample. On the other hand, by triggering more oxygen reactions in the form of O^{2-}/O^- in the bulk material, the lithium-ion diffusion was found to be much faster, which accounts for the high performance as well.

Since the activation of Li_2MnO_3 during the initial charge process is the main reason of the structural complexity in Li-rich NMC, preactivation of this phase during preparation is developed. Converting the surface of a Li-rich cathode material to an integrated layered ($R\bar{3}m$)—layered ($C2/m$)—spinel ($Fd\bar{3}m$) (LLS) composite phase is another important surface modification approach. Layered-spinel composite structures were initially proposed by Thackeray et al.^[109] It can be written as $x\text{Li}_2\text{MnO}_3 \cdot (1-x)\text{Li}_{1+y}\text{Mn}_{2-y}\text{O}_4$ ($0 < x < 1, 0 \leq y \leq 0.33$). The layered phase can achieve high capacity and the spinel phase can provide high rate-capability. The formation of cubic $\text{Li}_4\text{Mn}_5\text{O}_{12}$ from a net loss of Li_3O_6 from $3\text{Li}_2\text{MnO}_3$ has been extensively reported from reduction of the material surface via an ion exchange reaction.^[110] $\text{Li}_4\text{Mn}_5\text{O}_{12}$ is a type of spinel phase with a space group of $Fd\bar{3}m$, in which $1/3$ of the lithium ions reside in octahedral sites. The structural stability of this spinel phase enables the LLS material to possess outstanding performance without severe structure degradation.^[111] In other cases, reduction of lithium rich cathode materials has been shown to result in the partial formation of an artificial spinel phase on the surface that provides both lithium and electron conductivity.^[85,110,112] Figure 7 shows an example of the use of ALD to deposit a layer of AlPO_4 onto Li-rich NMC (HENMC), it was found that the surface Mn and Co underwent reduction reaction upon reaction with the trimethyl aluminum precursor, which was responsible for the formation of a spinel phase on the surface.

3.1.2. Surface Coating

The role of surface coating toward suppressing surface phase transition is a debated topic. Both CEI accumulation and O_2 release can lead to phase transitions on the surface. The use of an AlF_3 coating to increase structural stability is one of the few methods that have been reported to effectively

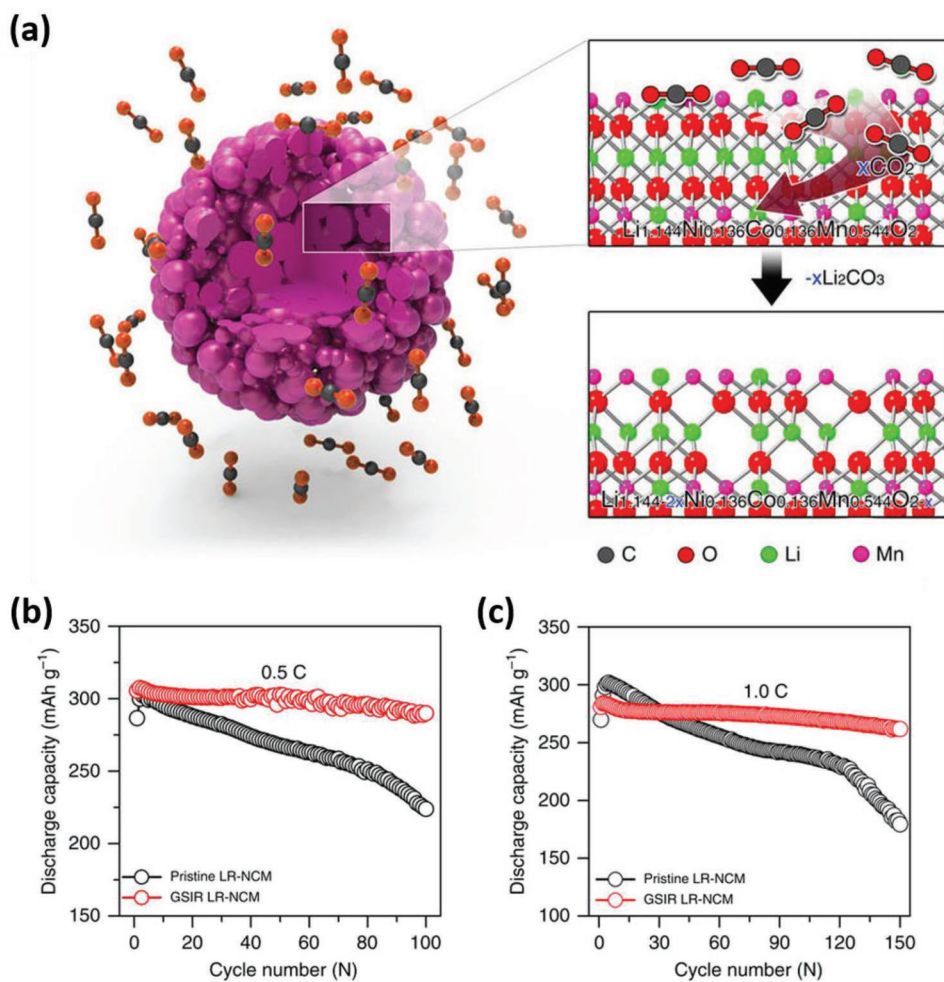


Figure 6. a) Schematic of GSIR between Li-rich layered oxides and carbon dioxide. b,c) Cycling performance of the pristine and GSIR LR-NCM at 55 °C by applying a constant current density of 0.5 C rate and 1.0 C rate (250 mA g⁻¹), respectively. Reproduced with permission.^[108] Copyright 2016, Springer Nature.

mitigate the transition from layered to spinel phase in Li-rich cathode materials by increasing the structural stability.^[113] A recent study by Wang's group provided visualized evidence toward the suppression of a layered to spinel phase transition in Al_2O_3 coated $\text{Li}_{1.2}\text{Ni}_{0.2}\text{Mn}_{0.6}\text{O}_2$ as shown in Figure 8. In a typical uncoated particle, the valence of Mn on the surface decreases after only 40 charge/discharge cycles, whereas the coated particles demonstrate a negligible surface Mn reduction. The uncoated particle also displays surface reconstruction with a depth of about 5 nm, however, the coated sample remained unchanged. In another study, the effect of sodium carboxymethyl cellulose (CMC) binder on the performance of $\text{Li}_{1.2}\text{Ni}_{0.13}\text{Co}_{0.13}\text{Mn}_{0.54}\text{O}_2$ was evaluated, which can also be regarded as a type of surface coating.^[114] The improvement was ascribed to three aspects, the stabilization of the active materials from delamination from the Al current collector, the suppression of voltage fade by the intercalation of Na^+ ions in the CMC binder through ion exchange and the inhibition of transition metal dissolution. While numerous studies have obtained mitigated phase transition results based on surface coating, discrepancy has also been reported by others. For the phase

transition that happened intrinsically within the cathode material itself, such as those induced by O_2 release in Li-rich NMC materials, surface coating effect was supposed to be marginal and the voltage fade problem cannot be efficiently addressed.^[115] In theory, surface phase changes that result from oxygen release is an intrinsic behavior, therefore simple coating is supposed to be not as effective in alleviating the phase transition that occur upon electrochemically cycling.^[115] Therefore, the role of surface coating is more complicated than it seems to be and hence more investigations are needed to better address the voltage fade problem.

3.2. Surface Modification as a Mechanical Buffer Layer

While there have been a tremendous amount of scientific reports published pertaining to coating materials aimed at suppressing mechanical cracks in anode, the same scientific investigation has not been adequately applied toward the cathode part. The surface modification required for an intergranular cracking surface should be able to accommodate the strain that

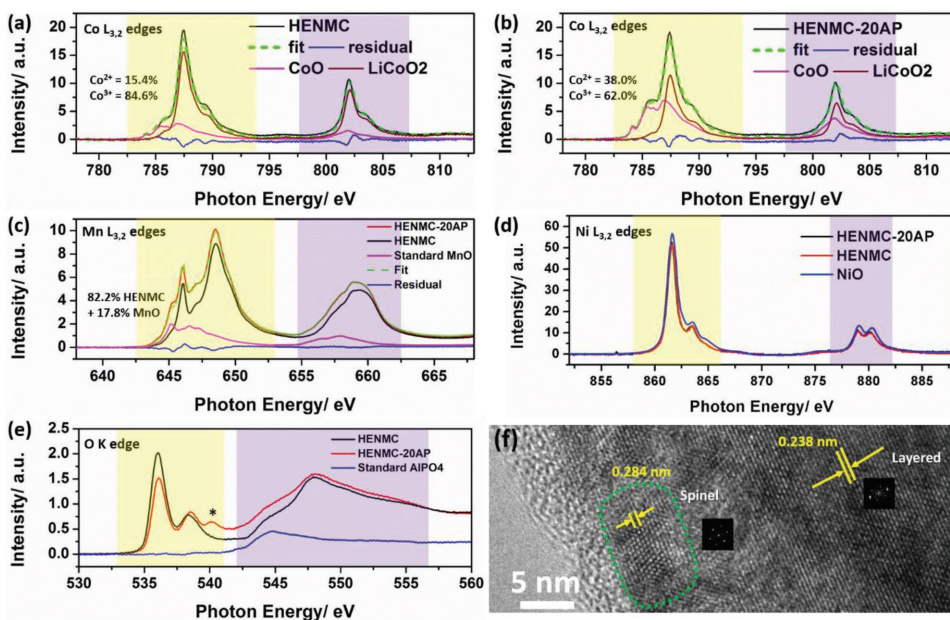


Figure 7. Soft XAS data of a) HENMC Co $L_{3,2}$ edges and b) HENMC-20AP Co $L_{3,2}$ edges fitted to standard CoO and LiCoO₂, the surface Co was reduced by 22.6% after ALD. c) Mn $L_{3,2}$ edges (the HENMC-20AP sample is fitted to the HENMC sample and standard MnO, the surface Mn was reduced by 17.8% after ALD). d) Ni $L_{3,2}$ edges (L_3 edges are marked with yellow color and L_2 edges are marked with purple color). e) O K edge (all of the XAS results in this figure are collected at total electron yield (TEY) mode). f) HRTEM image showing the different phases in the HENMC-20AP sample (inset: fast Fourier transform patterns). Reproduced with permission.^[114] Copyright 2017, Elsevier.

was generated upon electrochemical cycling. Grain boundaries within spherical secondary particles are regions where intergranular crackings happen predominantly, since liquid electrolyte may permeate into the gaps and ameliorate the side reaction. Approaches aimed at suppressing the cracks on these grain boundaries are limited, most often people work on the synthesis of more condense secondary particles. In a recent study, a Li₃PO₄ solid electrolyte was deposited onto a Ni-rich cathode material followed by heat-treatment as shown in **Figure 9**. The Li₃PO₄ solid electrolyte was found to have infused into the interior of the secondary particles and solidified on grain

boundaries, these solid electrolyte facilitates the lithium-ion diffusion across the grain boundaries. More importantly, as shown in **Figure 10b–e**, without the treatment, liquid electrolyte permeate into the gaps and facilitate the formation of intergranular cracks. On the other hand, the infusion of Li₃PO₄ was able to prevent the permeation of the liquid electrolyte and suppress side reactions from happening on the grain boundaries, which is essential to avoid intergranular crackings and achieve high performance.^[117]

Some metal oxides and fluorides such as Al₂O₃ and AlF₃ have been studied aimed at suppressing the crack formation inside of particles and were found to be effective.^[118] However, additional problems arise from coating materials as they are brittle and weak adhesion may result in film delamination, thereby diminishing performance. Taking this into consideration, polymers with better suited mechanical properties may be more ideal.^[119] Attempt on coating on anode materials aimed at suppressing cracks using self-healing polymers has been reported by Cui et al.^[120] Also, a molecular layer deposition (MLD) designed for polymer coating at the molecular level has been reported, this can be a potential method to adjust the cathode surfaces.^[121] In addition, since the primary reason for the cracking formation in cathode material stems from surface level phase transition, the strategies discussed previously may help to alleviate the occurrence of local cracking, as has been mentioned in the Li₃PO₄-infusion study.

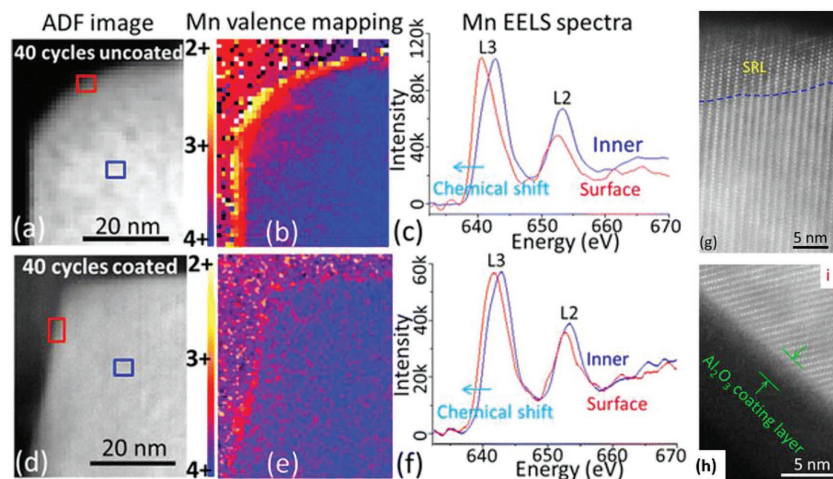


Figure 8. STEM-EELS study of Li_{1.2}Ni_{0.2}Mn_{0.6}O₂ and Al₂O₃ coated Li_{1.2}Ni_{0.2}Mn_{0.6}O₂ and their corresponding lattice images. Reproduced with permission.^[116] Copyright 2016, American Chemical Society.

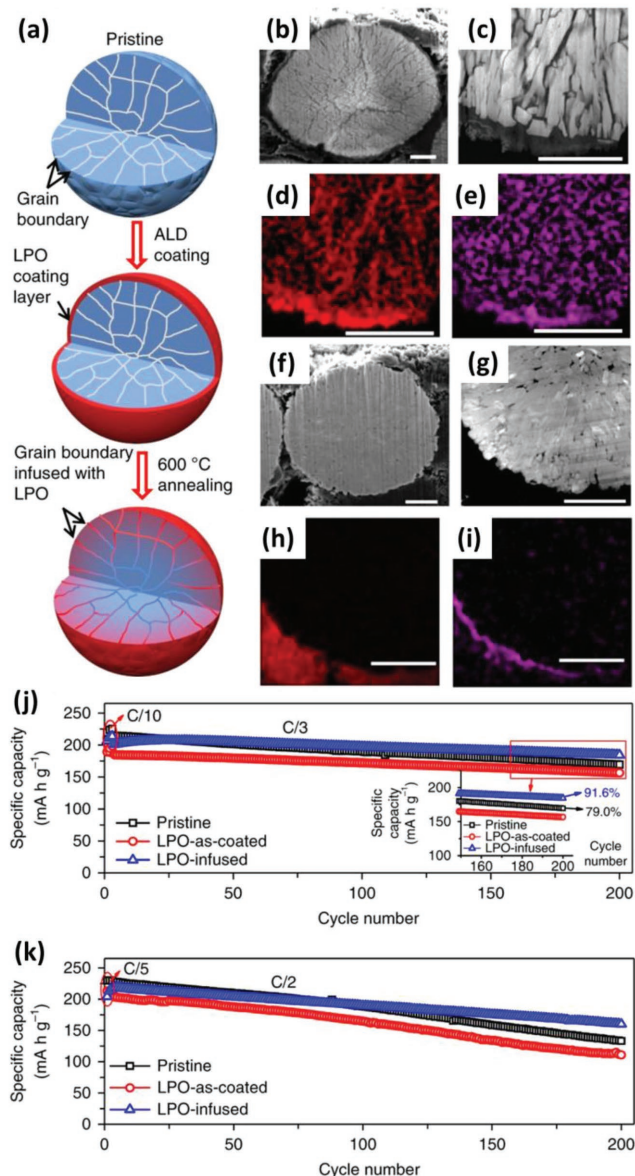
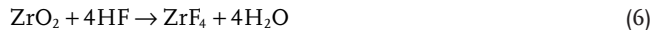


Figure 9. a) Schematic illustration of the ALD-derived Li₃PO₄ infusion process. b–e) Cross-section SEM image, STEM-HAADF image, C and F EDX mapping of a pristine Ni-rich cathode after 200 cycles. f–i) Cross-section SEM image, STEM-HAADF image, C and F EDX mapping of a Li₃PO₄-infused Ni-rich cathode after 200 cycles. j) Specific capacity retention after 200 cycles. k) Specific capacity as a function of cycle numbers when cycled at 60 °C. Reproduced with permission.^[117] Copyright 2018, Springer Nature.

3.3. Surface Modification as HF Scavenger

The use of surface modification techniques as an HF scavenger agent is quite straightforward. Metal oxides are often employed as surface coating materials in order to neutralize HF originated within the electrolyte as follows^[90,122]



More importantly, metal fluorides formed in these reactions are very stable in nonaqueous electrolytes and thus protect the cathode materials from further corrosion following complete consumption of the metal oxides.^[123] As a result, direct use of these metal fluorides, as well as metal phosphates, has been extensively reported owing to their stable nature.^[104,125]

As mentioned before, generation of HF in the electrolyte solution often results in transition metal dissolution. Additionally, transition metal reduction, in particular Mn, is often related to metal dissolution. A study from our group on ALD derived LiTaO₃ coated LiNi_{1/3}Mn_{1/3}Mn_{1/3}O₂ has demonstrated that transition metal dissolution can be suppressed by coating. The bare sample demonstrated 20 times higher transition metal dissolution than the sample with only 10 ALD cycles coating after 100 charge/discharge cycles.^[76] Another study conducted by our group explored the use of protecting LiNi_{0.5}Mn_{1.5}O₄ with atomic layer deposition derived FePO₄. Through the use of X-ray absorption spectroscopy, this study revealed that following electrochemical cycling, the use of surface coating can significantly affect the chemical state of Mn on the surface. Transition metal L_{3,2}-edge XAS measurements probe the unoccupied density of states for transition metal 3d and oxygen 2p bands, providing information of the oxidation state, spin state and metal oxide covalence.^[125] As shown in Figure 10a, following electrochemical cycling, the XAS data obtained for the Mn L_{3,2} edge XAS demonstrates an obvious peak shift toward lower energy. The uncoated samples display much less sharp peak at 646.5 eV as indicated by the red arrow. The higher intensity indicates that the Mn in the coated sample are at higher oxidation state after cycling. Figure 10b shows the stability tests, the sample with higher final Mn oxidation state demonstrates much less intense capacity fade. Therefore, surface coating is effective in suppressing the Mn reduction and subsequent dissolution. A prelithiation method that enables electrolyte reduction reaction manually by charging the cell from relatively lower voltage was reported by Wu and co-workers.^[126] They found that the process generates a desirable CEI layer and provided ample protection for NMC532/CNTs composites from metal dissolution.

3.4. Metal–Oxygen Bond Stabilization via Surface Modification

The dissolution of transition metals originates from the cleavage of metal–oxygen bonds. Therefore attempts aimed at strengthening this bond at the surface are one strategy to prevent transition metal dissolution from occurring. A regular coating diminishes the contact between the cathode materials and the electrolyte to prevent metal dissolution. The electron and ion diffusion is, however, restricted by the coating material. Numerous investigations have reported using a doping method to avoid the insulating effect of coating materials. However, concerns regarding the loss of active components in the cathode

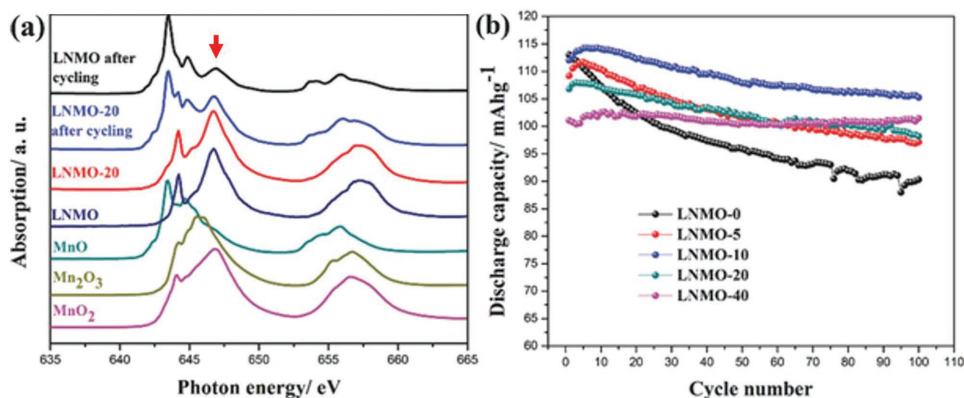


Figure 10. a) XAS results of different LNMO samples and standard manganese oxides. b) Cyclic stability tests of LNMO with various FePO_4 coating thicknesses. Reproduced with permission.^[127] Copyright 2014, Wiley-VCH.

materials arise when it comes to the bulk scale. The principle of surface doping design is more effective in this regard. Surface doping uses two principles to suppress metal dissolution. The first one is the stabilization of the metal–oxygen bond and the second one is to minimize the amount of susceptible metal ions without affecting structural integrity.

Synchrotron soft XAS was used to study the role of Mg on $\text{LiNi}_{0.5}\text{Mn}_{1.5}\text{O}_4$ cathode material by probing the transition metal $L_{3,2}$ -edges and oxygen K-edge.^[128] The $\text{LiNi}_{0.5}\text{Mn}_{1.5}\text{O}_4$ was charged to a voltage as high as 5 V and shown to undergo very intensive chemical alteration centered around the Ni–O bond as it becomes highly oxidized and is forced into an unstable state that is prone to be reduced by the electrolyte. These experiments revealed the existence of a new Ni–O bond due to electron depletion for Mg doped surface with peak intensity ratio changing for both Ni $L_{3,2}$ -edges and O K-edge in the surface sensitive total electron yield (TEY) spectra, suggesting that Mg doped surfaces retain a more oxidized surface upon electrochemical cycling. As a result, a more robust Ni–O bond is formed and adversely resists electrolyte reduction. It is worthwhile to note that this research was focused primarily on the state of the Ni–O bond. Additional studies should be performed at the Mn $L_{3,2}$ edges since the reduction of surface Mn, and subsequent Jahn-Teller distortion effect can be tracked. The combination of these observations present important guidelines for principle through which surface doping aids in the stabilization of metal–oxygen bonds.

The mechanism through which surface doping design works also involves the replacement of soluble metal ions on the surface, as has been mentioned before. A representative example is the formation $\text{LiCo}_{1-x}\text{Al}_x\text{O}_2$ solid solution on the surface of LiCoO_2 cathode material. Previous discussions have mentioned the role of Al in suppressing surface phase transition in LiCoO_2 . The incorporation of Al as an insoluble source in nonaqueous electrolyte has been shown to also reduce the dissolution of Co. The fundamental principle was presented by Dahéron and coworkers in 2009.^[129] They tracked surface acid-base properties of the $\text{LiCo}_{1-x}\text{Al}_x\text{O}_2$ while adjusting the value of x . To be more specific, NH_3 and SO_2 gases were adsorbed onto the surface of $\text{LiCo}_{1-x}\text{Al}_x\text{O}_2$. Depending on the way the N and S are bonded on the Lewis acidic sites, Lewis basic sites and Brønsted acidic sites, different binding energies for N 1s and S

2p could be identified by XPS. The results showed that surface basicity drops drastically with the incorporation of Al into the surface to form solid solution. The lower basicity the surface is, the less vulnerable it is to be etched by HF.

3.5. Surface Modification as Electronic/ Li^+ Conductivity Facilitator

Surface coating does not change the inherent electronic and lithium-ion conductivity of cathode materials, it actually provides conducting network among individual particles so as to guarantee consecutive mobile channels to maximize the utilization of active materials. The way through which surface modification enables enhanced performance is highly dependent on the properties of the materials and how they are deposited.

3.5.1. In Situ Deposition of Electronic Conductivity Facilitators

The first category of the coating materials involves the substances that are intrinsically electronically conductive. Metals such as Ag, Cu and Al have been studied, but their high cost is not acceptable for mass productions. Furthermore, deposition of metallic coatings often form incoherent films that do not completely cover the surface of the active particle. Additionally, the acidic nature of the electrolyte will dissolve the metallic coating and cause further contamination to the active materials.^[130] Similarly, coating some compounds that possess considerable electronic conductivity such as TiN and RuO_2 is also feasible regardless of the cost.^[131] Rutile TiO_2 is another possible carbon-free coating material that can promote electrical conductivity and has been reported as a coating for $\text{Li}_4\text{Ti}_5\text{O}_{12}$ by Wang et al.^[132]

Alternatively, the in situ growth of conductive polymers has been widely reported. Polymers such as polyaniline (PANi), polypropylene (PPy), polythiophene (PT), poly(3,4-ethylenedioxythiophene) (PEDOT), polyimide have been employed as electronic conductive coatings for cathode materials.^[119,133] The benefit of in situ grown polymers is that monomers can be easily nucleated on the surface of powders and become polymerized through the use of catalyst, thereby forming coatings with uniform thickness. However, for cathode

materials that operate at high voltage, the electrochemical stability of the coated polymer should be taken into consideration.

Carbon-based materials such as graphene, carbon nanotubes (CNTs), graphite and amorphous carbon have also been employed to form composites with the cathode materials. These carbon-based materials generally help construct a 3-D conductive network as opposed to a traditional conductive coating. For materials that do not suffer from dissolution, such as LiFePO_4 , using graphene or CNTs to form composites an effective strategy toward improving the electronic conductivity.^[134] Song and coworkers used a high speed ball milling method to tether very thin and porous graphite layers onto LiMn_2O_4 . Their studies revealed that this conformal layer can double the capacity of LiMn_2O_4 , as shown in Figure 11a,b.^[135] Besides, a novel concept of hybrid coating, i.e., a composite coating layer that contains both electronic and lithium conductive substances has been reported, Figure 11c–e shows the mechanism of the hybrid coating. In this study, a coating layer that is composed of Li_3PO_4 and carbon has been investigated, with this type of coating, conductivity and surface stability can be enhanced simultaneously. Therefore the performance of the sample with hybrid coating was significantly improved.

Another category for enhancement of performance by surface modification is the deposition of lithium conductive

coatings. Compounds that are often considered as candidates for solid state electrolyte such as LiAlO_2 , Li_2ZrO_3 , Li_3PO_4 , LaPO_4 , Lipon, lithium boron oxide glass, LiTaO_3 et al. have been utilized in order to facilitate transfer of lithium ions at the surface of cathode materials.^[137–142]

3.5.2. Deposition of Conductivity Facilitators via Post-treatment

Pyrolysis of carbon containing organics via a solid state method or chemical vapor deposition method has been a proven strategy to improve the performance of cathode materials, particularly for materials with poor intrinsic electronic conductivity and are resistant to reduction, such as LiFePO_4 and LiMnPO_4 , and has been comprehensively reviewed by our group.^[143] Carbon coating for LiMeO_x (Me = Ni, Mn, Co, etc.), however, remains a major challenge due to the oxidation nature of the metal oxides, which will be reduced by carbon under high temperature and often resulting in diminished performance. Many researchers have attempted to achieve pyrolysis of organic carbon at temperatures as low as 350°C in a short time so as not to burn up the carbon, the feasibility of this method is under debate.^[135,144]

Methods employing surface doping is another strategy to increase surface ionic conductivity. For example,

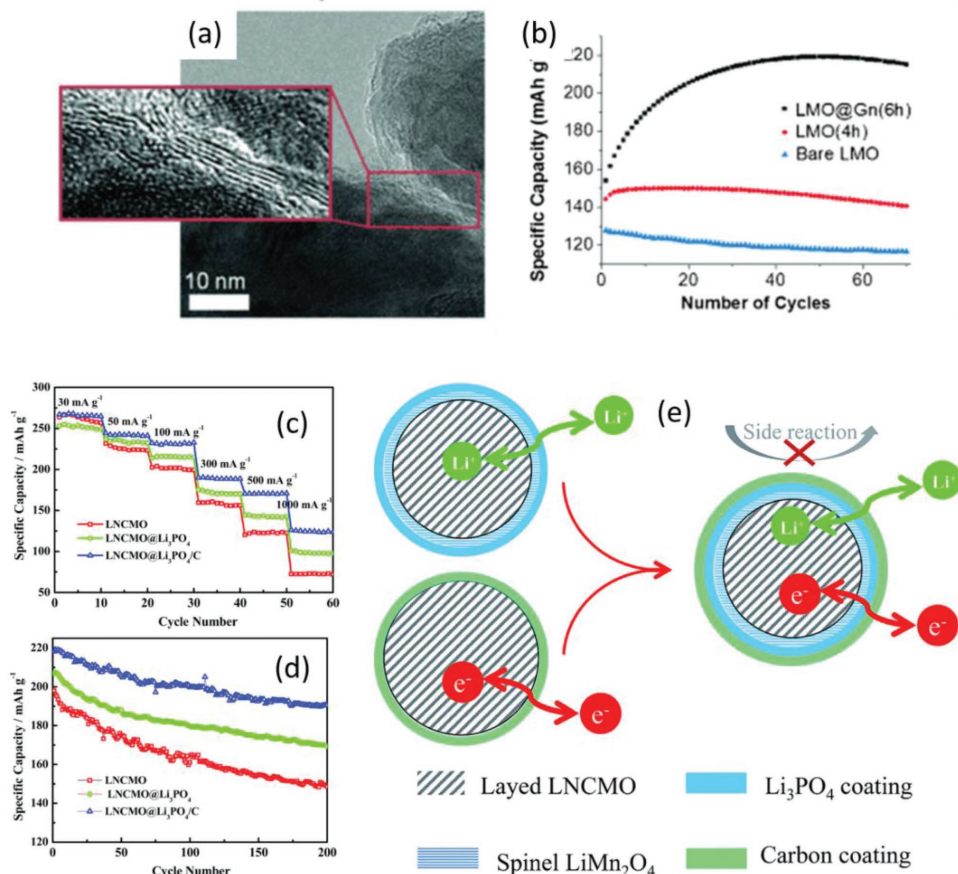


Figure 11. a) Porous Graphite coating of LiMn_2O_4 . b) Discharge capacity of porous graphite coated LiMn_2O_4 with a voltage range of 2.4–4.3 V. Reproduced with permission.^[135] Copyright 2014, Wiley-VCH. c) Rate capability test and d) stability test of the LNCMO, Li_3PO_4 coated LNCMO, and $\text{Li}_3\text{PO}_4/\text{C}$ coated LNCMO. e) Mechanism of the hybrid coating. Reproduced with permission.^[136] Copyright 2015, Royal Society of Chemistry.

Manthiram et al.^[145] coated 5 V class cathode material $\text{LiMn}_{1.42}\text{Ni}_{0.42}\text{Co}_{0.16}\text{O}_4$ with Al_2O_3 followed by heating at 400–600 °C for 3 h. Despite the insulating nature of Al_2O_3 , Al_2O_3 was found to react with the cathode surface during annealing resulting in the formation of LiAlO_2 , which is a good lithium conductor. Similar behavior was also observed by Zhang et al.^[146] in their attempt toward coating $\text{Li}(\text{Ni}_{1/3}\text{Co}_{1/3}\text{Mn}_{1/3})\text{O}_2$ with ZrO_2 via post annealing of $\text{ZrO}(\text{NO}_3)_2$. Near surface Zr was found to exist in the form of Li_2ZrO_3 , which is also a good lithium conductor. In a more complicated case, as shown in **Figure 12**, Yang et al.^[147] found that utilizing a AlPO_4 coating on LiCoO_2 , followed by heat treatment, gave rise to a dual phase of $\text{LiCo}_{1-y}\text{Al}_y\text{O}_2$ at the ≈ 10 nm region and Li_3PO_4 at ≈ 100 nm region near the surface due to Li_2CO_3 reacting with the AlPO_4 . The layer of $\text{LiCo}_{1-y}\text{Al}_y\text{O}_2$ was found to effectively suppress metal dissolution while Li_3PO_4 improves lithium-ion diffusion. The presence of Li_3PO_4 is one reason why AlPO_4 is more effective than Al_2O_3 in improving the capacity retention of LiCoO_2 especially at extended voltage ranges.

3.5.3. Formation of Conductivity Facilitators during Lithiation/Delithiation

When the surface coating material can accommodate reversible insertion/desertion reaction of lithium ions, they tend to turn into good lithium facilitators. For example, Ta_2O_5 has been reported to undergo the following reaction when cycled^[148]



At reduced dimensions, LiTaO_3 is a favorable solid-state electrolyte. Heitjans et al.^[149] proved that the LiTaO_3 with a particles

size of 20 nm demonstrates a lithium-ion conductivity of about $3 \times 10^{-6} \text{ S cm}^{-1}$. Our group has successfully synthesized conformal LiTaO_3 film via atomic layered deposition through a combination of Li_2O and Ta_2O_5 deposition subcycles.^[76]

TiO_2 is another widely studied coating material that can be reversibly lithiated/delithiated under the appropriate voltage range. The resulting lithiated LiTiO_2 , has indeed been shown to be a good electron conductor with poor lithium-ion conductivity, which has been theoretically proven by Wagemaker et al.^[150]

In an attempt to theoretically predict the criteria of screening coating materials, Wolverton and co-workers calculated the lithiation enthalpies required for cathode coating materials, such as metal oxides and metal fluorides. By assuming the overall conversion reaction of metal oxides and metal fluorides as



respectively, they calculated the density function theory (DFT) voltages of oxides and fluorides compared to the experimental voltages, as shown in **Figure 13**. The higher the lithiation voltage, the more likely the coating gets lithiated during electrochemical cycling. It can be seen that fluorides generally have much higher lithiation voltage compared to oxides. This phenomenon can be attested to the increased electronegativity of fluorine compared to oxygen. This study illustrates the importance of screening methods when selecting appropriate coating materials.

3.6. Surface Modification to Shield the Cathode Material from CO_2 and Water

Using surface modifications to protect the surface from reacting with CO_2 and water is quite straightforward. In theory, any of the aforementioned methods that can generate a layer of material stable in CO_2 and water can achieve this goal. However,

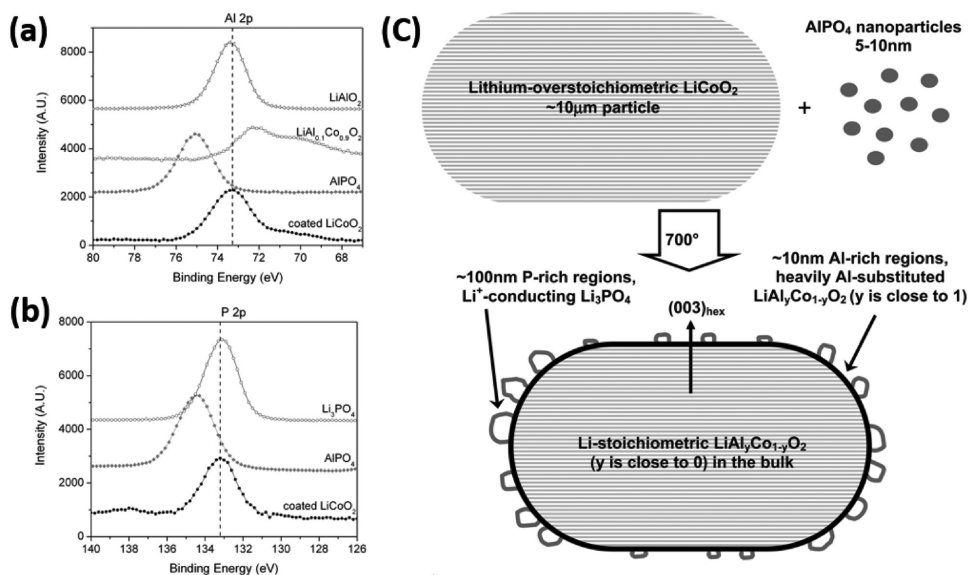


Figure 12. XPS spectra of a) Al 2p and b) P 2p of AlPO_4 coated LiCoO_2 ; c) schematic illustration of the AlPO_4 surface modification mechanism. Reproduced with permission.^[147] Copyright 2007, American Chemical Society.

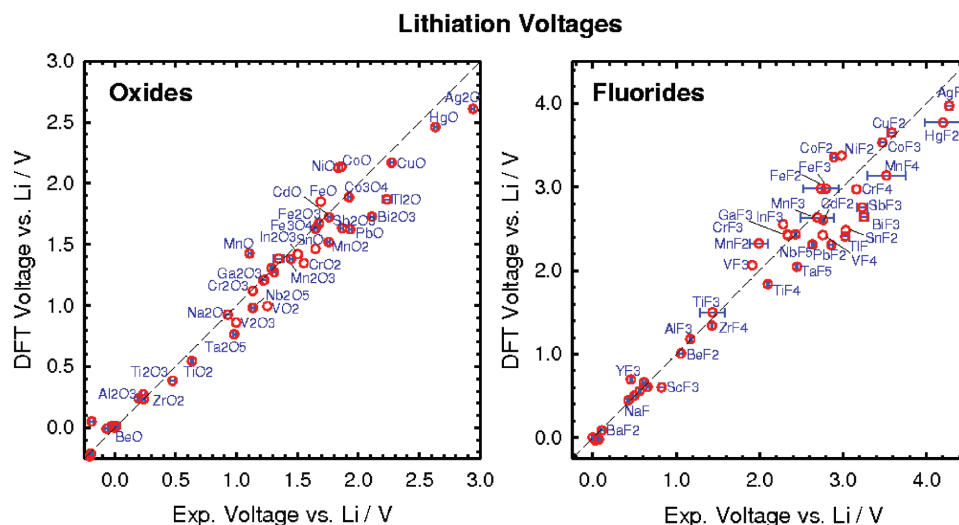


Figure 13. Calculated average voltages for oxides and fluorides versus voltages estimated from experimental formation enthalpies. Reproduced with permission.^[151] Copyright 2014, Wiley-VCH.

a complete protection requires the layer to be uniform with full coverage. In many cases, the material was subject to bulk doping or concentration gradient (lower Ni³⁺ on the surface) designs,^[152] these are pertinent to bulk modifications and will not be elaborated in this review. Surface coating has been utilized to address this challenge. Oh et al. coated the Ni-rich LiNi_{0.7}Co_{0.15}Mn_{0.15}O₂ with spinel LiMn_{1.9}Al_{0.1}O₄ and found that it can maintain high capacity even after long-time storage in air.^[153] In a more detailed study, Chen et al. adopted a dual-conductive coating comprised of polypyrrole (PPy) and Li₃PO₄ to protect the LiNi_{0.7}Co_{0.15}Mn_{0.15}O₂, in the coating process, (NH₄)₂HPO₄ was used as the source of PO₄³⁻ without further addition of lithium sources, it reacts with the Li₂CO₃ and LiOH impurities on the cathode material surface and forms insoluble and ionically conductive Li₃PO₄. PH values of the pristine and coated samples were found to be 11.97 and 10.81, respectively, which is attributed to the consumption of lithium residuals and protective role of PPy.^[154]

4. Surface Modification Methods

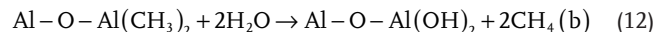
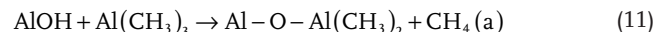
4.1. Conventional Methods

Conventional surface modification techniques are often realized from methods that are easily achievable such as sol-gel, solid state reaction, pulsed laser deposition, chemical vapor deposition (CVD) and so on. The basic experimental steps of these methods are depicted in **Figure 14**, Cho et al. have also summarized these techniques in their recent progress report.^[155] However, regardless of the scalability and effectiveness, the films yielded from these conventional techniques are always lack of controllability on thickness and uniformity.^[156] A table of typical coating materials on typical cathodes is listed in **Table 1**. It can be seen that metal oxides, phosphates, fluorides, solid-state electrolyte, polymer and carbon are the major coating materials. A great deal of efforts have been devoted to investigating coating materials for cathode materials but

unfortunately, lots of them are simply reporting this observation without attempting to understand the underlying mechanism rooted in the cathode material surface.

4.2. Atomic Layer Deposition

Atomic layer deposition (ALD) is a technique used to fabricate conformal coatings with controlled thickness. Using the widely applied Al₂O₃ as an example, a representative schematic of the ALD process is shown in **Figure 15a**. In a typical ALD process, the surface of the substrate is initially functionalized with hydroxyl groups, and a saturating dose of trimethylaluminum (TMA) is pulsed in and purged out. This is subsequently followed by a saturating dose of H₂O that is purged and byproducts are also purged out. The surface reactions occur as follows:



Each of these reactions represents a half reaction and provides the unique advantage of enabling the self-limited growth, i.e., deposition in a controllable manner. In addition, the bottom-up growth employed by ALD allows for ultrauniform and conformal deposition.^[142,174]

Though the development of ALD has been several decades, its application in lithium-ion batteries is not long.^[175] The application of ALD in battery materials has been extensively reviewed by our group.^[176,177] **Table 2** summarizes the reported ALD derived surface modifications for cathode materials. In addition, direct synthesis of cathode materials via ALD has been investigated recently, and provides a route toward the enablement of ultrathin flexible batteries.^[178] Nevertheless, ALD is found to have restrictions at a technical

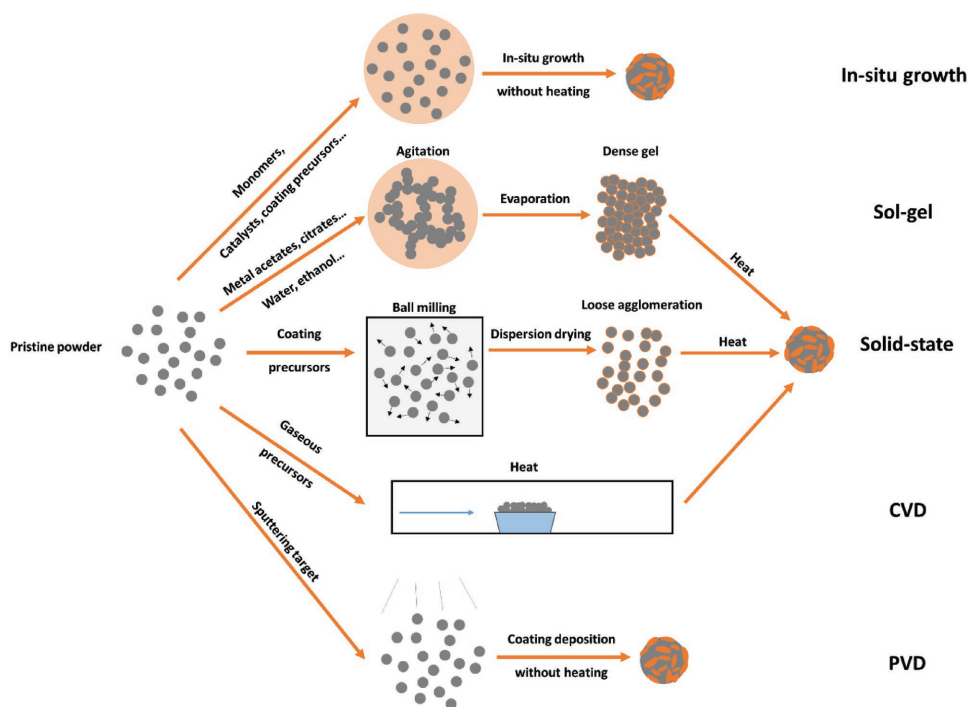


Figure 14. Schematic diagram summarizing conventional coating techniques.

Table 1. Conventional coatings for cathode materials (LCO: LiCoO_2 , NCM: $\text{Li}_{1+n}\text{Ni}_x\text{Co}_y\text{Mn}_{1-x-y-n}\text{O}_2$, LNMO: $\text{LiNi}_{0.5}\text{Mn}_{1.5}\text{O}_4$, LMO: LiMn_2O_4).

| Base material | Coating material | Experimental | Test condition | Performance | Note | Ref. |
|---------------|--|---|--------------------------------------|--|--|-------|
| LCO | $\text{LiAlO}_2/\text{Al}_2\text{O}_3$ | $(\text{C}_9\text{H}_{21}\text{O}_3)\text{Al}$ LiOH 600 °C 3 h | 2.8–4.3 V, 0.1 C | 98.4% capacity retention after 20 cycles using LiAlO_2 coating | Ionically conductive LiAlO_2 favors better kinetics than Al_2O_3 | [157] |
| | $\text{Y}_3\text{Al}_5\text{O}_{12}$ (YAG) | $\text{Al}(\text{OC}_4\text{H}_9)_4$ 723K 823K 923K 5 h | 2.75–4.4 V, 0.2 C | Seven times more stable than pristine LiCoO_2 | Prevents rapid increase in impedance | [140] |
| | FePO_4 | $\text{Fe}(\text{NO}_3)_3$ $(\text{NH}_4)_2\text{HPO}_4$ 550 °C 10 h | 2.75–4.3 V, 1 C | 90.6% capacity retention compared with 72.5% for pristine sample after 400 cycles | Restrains the impedance growth of the LiCoO_2 | [158] |
| | Polyimide/C | Polyamic acid, sucrose Temperature ramp up to 400 °C under N_2 | 3.0–4.4 V, 1 C | 87% capacity retention compared with 42% for pristine sample after 50 cycles | Polyimide is lithium-ion conductive, a synergistic coating provides both high conductivity and protection | [159] |
| | AlF_3 | NH_4F $\text{Al}(\text{NO}_3)_3$ 400 °C 5 h | 3.0–4.5 V, 20 mA g^{-1} | 98% capacity retention compared with 17% for pristine sample after 50 cycles | Decrease charge transfer resistance and prevents Co dissolution by reducing the formation of LiF | [160] |
| NCM | MnO_2 | MnSO_4 900 °C 12 h | 2.0–4.8 V, 0.2 C | 94.5% capacity retention compared with 91.5% for pristine, increased capacity and coulombic efficiency | Suppresses CEI formation | [161] |
| | Metal–organic frameworks (MOF) | MnCl_2 , 2,5-dihydroxyterephthalic acid 200 °C 5 h | 2.0–4.75 V, 30 mA g^{-1} | Over 300 mAh g^{-1} discharge capacity and 91.1% Coulombic efficiency was obtained | Porous structure of MOF can absorb released oxygen. | [162] |
| | AlF_3 | $\text{Al}(\text{NO}_3)_3$ NH_4F 400 °C 5 h | 2.0–4.6 V, 24 mA g^{-1} | 91.6% capacity retention compared with 73.4% for the pristine electrode | Facilitates the Li chemical leaching and improved the initial Li_2MnO_3 layer transformation to spinel phase | [103] |

Table 1. Continued.

| Base material | Coating material | Experimental | Test condition | Performance | Note | Ref. |
|---------------|---|--|---------------------------------------|--|--|-------|
| | Al ₂ O ₃ + LiF | Al(NO ₃) ₃ , NH ₄ F 400 °C 5 h | 2.0–4.8 V, 1 C | Initial discharge capacity was 15 mAh g ⁻¹ larger than bare sample. | The dual coating simultaneously promotes the chemical stability and electrochemical performance simultaneously | [163] |
| | Gradient Li(Ni _{0.46} Co _{0.23} Mn _{0.31}) O ₂ | Ni-deficiency solution feed, 780 °C 20 h | 2.0–4.4 V, 0.5 C | 96.5% capacity retention compared with 80.4% for the pristine electrode | Concentration-gradient from surface to bulk stabilizes the cathode | [32] |
| | Li ₂ ZrO ₃ | Zr(NO ₃) ₄ CH ₃ COOLi 650 °C 5 h | 2.5–4.8 V, 0.1 C | 89% capacity retention compared with 77% for the pristine electrode | Stabilizes the crystal structure and increases lithium-ion diffusion | [137] |
| | Al ₂ O ₃ + RuO ₂ | Al(NO ₃) ₃ RuCl ₃ 450 °C 3 h | 2.0–4.6 V, 0.05 C | 60% capacity retention compared with 40% for the pristine electrode when cycled from C/20 to 5C rate | Suppresses oxygen evolution and electrolyte decomposition, RuO ₂ provides good electronic conductivity | [164] |
| | LiNi _{0.5} Mn _{1.5} O ₄ | LiAc Mn(Ac) ₂ Ni(Ac) ₂ 500 °C 5 h | 2.0–4.8 V, 5 C | 94.4% capacity retention compared with 58.6% for the pristine electrode at 5C | Protects the cathode from the electrolyte and facilitates lithium-ion transportation | [165] |
| LNMO | Li ₃ PO ₄ | 760 °C 200 h | 3.0–5.0 V, 5 C | 80% capacity retention after 650 cycles compared with 20% after 250 cycles without coating | Minimizes decomposition of electrolyte and prevents ordered crystal structure growth | [141] |
| | SiO ₂ with reactive vinyl groups | Vinyltrimethoxysilane NH ₄ OH 110 °C 12 h | 3.0–4.9 V, 0.5 C | Up to 83.9% capacity retention compared with 77.0% for pristine sample after 100 cycles | Vinyl groups on SiO ₂ form cross-linking sites and better protect the electrode | [166] |
| | LiAlO ₂ | Aluminum isopropoxide Li ₂ CO ₃ 900 °C 15 h | 3.5–5.0 V, 0.1 C | Increased stability especially at high temperature operation | Strengthened by the Al incorporated into the surface provides a stable interface | [139] |
| | Polyimide | Stepwise imidization of polyamic under nitrogen | 3.5–5.0 V, 1 C | 120 mAh g ⁻¹ capacity compared with only 98 mAh g ⁻¹ for pristine sample after 50 cycles | Polyimide is ion-conductive, it pro- vides continuous surface coverage and retards the Mn dissolution | [167] |
| | BiOF | Bi(NO ₃) ₃ NH ₄ F 450 °C 5 h | 3.5–5.0 V, 1 C | 114.1 mAh g ⁻¹ capacity compared with only 41.4 mAh g ⁻¹ for pristine sample after 70 cycles under 55 °C | BiOF nanolayer is an HF scavenger. Also inhibits the metal dissolution | [168] |
| LMO | graphene | Liquid-polyacrylonitrile | 3.5–4.4 V, 100 mA cm ⁻³ | Significantly improved discharge capacity and stability | Graphene-like coating suppresses Mn dissolution and decreases the impedance | [169] |
| | FeF ₃ | Fe(NO ₃) ₃ NH ₄ F 400 °C 5 h | 3.5–4.2 V, 0.2 C | Up to 68.2% capacity retention compared with 42.5% for pristine sample | The FeF ₃ coating suppresses Mn dissolution, impedance growth and improves the thermal stability | [170] |
| | FePO ₄ | Fe(NO ₃) ₃ (NH ₄) ₂ HPO ₄ 400 °C 6 h | 3.5–4.3 V, 0.2 C | Up to 68% capacity retention com- pared with 45% for pristine sample | The FePO ₄ separates the electrolyte and increases the conductivity of the CEI layer | [171] |
| | [Li,La]TiO ₃ | La(NO ₃) ₃ Ti(OC ₄ H ₉) ₄ 400 °C 5 h | 3.0–4.2 V, 30 mA g ⁻¹ | Up to 87% capacity retention com- pared with 37% for pristine sample | [Li,La]TiO ₃ stabilizes the surface and suppresses the growth of impedance | [172] |
| | V ₂ O ₅ | Acetyl acetone vanadium 400 °C 2 h | 3.0–4.5 V, 2 C | Up to 92.82% capacity retention compared with 75.08% for pristine sample under 2 C | V ₂ O ₅ provides both good lithium and electrical conductivity and stabilize the surface | [173] |

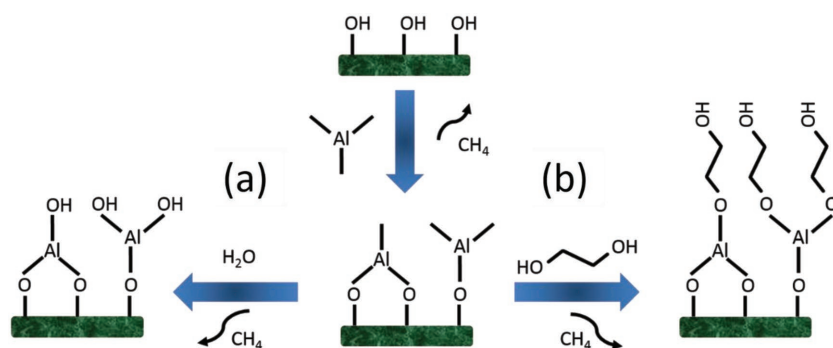


Figure 15. Schematic illustration of a) ALD process of Al_2O_3 synthesis and b) MLD process for deposition of alucone.

view. Lee et al.^[179] found that when Al_2O_3 was directly deposited onto the cathode material LiCoO_2 powders, the conformal but insulating Al_2O_3 will block the transportation of lithium ions and electrons seriously. Alternatively, the Al_2O_3 deposited onto as-prepared electrode sheets was found to be much more effective. Another way to avoid the severe impedance of ALD coating on powders is postannealing, as has been found in our recent study, postannealing the TiO_2 coated $\text{LiNi}_{0.5}\text{Mn}_{1.5}\text{O}_4$ can bolster the capacity with a value of 30% without the loss of stability compared to simply TiO_2 coated

Table 2. ALD derived coatings on cathode materials.

| Coating material | Base material | Experimental conditions | Substrate | Note | Ref. |
|-------------------------|---|--|--------------------|--|---------------|
| Al_2O_3 | LiCoO_2 | Trimethylaluminum H_2O 180°C | Powder | Capacity drops nearly to zero when ALD cycle number increases to only 10 | [183] |
| | LiCoO_2 | Trimethylaluminum H_2O 180°C | Electrode | ALD on electrodes undermines the insulation on conductive carbon | [182] |
| | LiCoO_2 | Trimethylaluminum H_2O 120°C | Electrode | Al_2O_3 does not grow on binders without hydroxyl functional group | [184] |
| | LiCoO_2 | Trimethylaluminum H_2O 180°C | Electrode | Exceptionally high durability with 250% improvement | [185] |
| | LiCoO_2 | Trimethylaluminum H_2O $<120^\circ\text{C}$ | Electrode | Impedes the redox current at the cathode surface | [186] |
| | LiCoO_2 | Trimethylaluminum H_2O 180°C | Powder | Reduces the interfacial resistance development between the cathode and solid state electrolyte | [187] |
| | LiMn_2O_4 | Trimethylaluminum H_2O 120°C | Electrode | Reduces the dissolution rate of Mn, 10 ALD cycle number shows best performance | [188] |
| | $\text{LiNi}_{1/3}\text{Mn}_{1/3}\text{Co}_{1/3}\text{O}_2$ | Trimethylaluminum H_2O 180°C | Powder | 4 ALD cycle of Al_2O_3 provides great help without losing conductivity | [189] |
| | | Trimethylaluminum H_2O 180°C | Powder + Electrode | Heat treatment on electrode can result in enhanced lithium-ion conductive surface | [190] |
| | $\text{LiNi}_{0.5}\text{Mn}_{1.5}\text{O}_4$ | Trimethylaluminum H_2O 90°C | Electrode | The Al_2O_3 coating effectively suppresses the formation of Mn^{2+} . | [191] |
| ZrO_2 | LiMn_2O_4 | Zirconium tert-butoxide H_2O 120°C | Powder | Epitaxial growth of ZrO_2 was observed after annealing the ZrO_2 coated sample | [109,192,193] |
| ZnO | $\text{LiNi}_{0.5}\text{Co}_{0.2}\text{Mn}_{0.3}\text{O}_2$ | Diethylzinc H_2O 100°C | Powder | The ultrathin ZnO does not block lithium-ion diffusion | [194] |
| | LiMn_2O_4 | Diethylzinc H_2O 120°C | Powder + Electrode | ZnO coating can improve the performance especially at high temperature | [193,195] |

Table 2. Continued.

| Coating material | Base material | Experimental conditions | Substrate | Note | Ref. |
|---------------------------------|---|---|-----------|---|-----------|
| TiO ₂ | LiCoO ₂ | Titanium isopropoxide H ₂ O <120 °C | Electrode | Conformal TiO ₂ coating may decompose and fail to protect the cathode | [186,196] |
| MgO | LiNi _{0.5} Co _{0.2} Mn _{0.3} O ₂ | Bis(ethylcyclopentadienyl) magnesium H ₂ O 200 °C | Powder | MgO coated cathode shows improved energy retention compared to ZrO ₂ coating and reduced overpotential compared to Al ₂ O ₃ coating. | [197] |
| LiAlO ₂ | LiNi _{0.5} Mn _{1.5} O ₄ | Trimethylaluminum Lithium tert-butoxide H ₂ O 225 °C | Electrode | LiAlO ₂ as a lithium conductor prohibits transitional metal deposition on the graphite counterpart | [198] |
| LiTaO ₃ | LiNi _{1/3} Mn _{1/3} Co _{1/3} O ₂ | Tantalum ethoxide Lithium tert-butoxide H ₂ O 225 °C | Electrode | LiTaO ₃ as a solid state electrolyte improves the performance of NMC especially at expanded voltage region | [120] |
| FePO ₄ | LiNi _{0.5} Mn _{1.5} O ₄ | Trimethylphosphate Ferrocene H ₂ O 130 °C/75 °C | Powder | Amorphous FePO ₄ can accommodate Li ⁺ and enables fast Li ⁺ transportation | [123] |
| AlPO ₄ | | Trimethylaluminum Trimethylphosphate H ₂ O 250 °C | Powder | Alters the surface structure and suppresses the O ₂ release | [107] |
| | LiNi _{0.5} Mn _{1.5} O ₄ | Trimethylaluminum Trimethylphosphate H ₂ O 250 °C | Powder | The coating suppresses the transition metal dissolution and enhances the thermal stability. | [199] |
| MgF ₂ | LiNi _{0.5} Mn _{1.5} O ₄ | Hexafluoroacetylacetone Bis(ethylcyclopentadienyl)-magnesium 275 °C | Powder | Prevents the excessive formation of byproducts | [200] |
| AlW _x F _y | LiCoO ₂ | Tungsten hexafluoride Trimethylaluminum 200 °C | Powder | This film allows for chemical inertness of AlF ₃ and high electrical conductivity of a metal | [201] |
| LiAlF ₄ | LiNi _{0.8} Mn _{0.1} Co _{0.1} O ₂ | lithium tert-butoxide Titanium tetrafluoride Aluminum trichloride 250 °C | Electrode | LiAlF ₄ is stable and lithium conductive | [202] |
| Li ₃ PO ₄ | LiNi _{0.76} Mn _{0.14} Co _{0.10} O ₂ | lithium tert-butoxide Trimethylphosphate 300 °C | Powder | The post-annealing treatment allowed for Li ₃ PO ₄ infusion, which protected the grain boundaries from cracking. | [85] |

LiNi_{0.5}Mn_{1.5}O₄.^[96] The reason for this difference is schematically shown in **Figure 16**. Another good example is the infusion mechanism as has been introduced in Figure 10. This method solves the surface phase transition, electrolyte decomposition and intergranular cracking simultaneously.^[117] These studies remind us that the conformal nature of ALD has special requirement on the coating material and the substrate. In other words, if the coating material is insulating, deposition on electrode is preferred, but concerns regarding the binder decomposition at elevated deposition temperatures arise. On the other hand, direct deposition on powders is feasible only when the coating is extremely thin or the coating material is conductive. In this respect, developing binders with high thermal stability and coatings with high conductivity is the primary future direction for ALD on cathode materials.

4.3. Molecular Layer Deposition

Molecular layer deposition (MLD) is another technique analogous to ALD, in which an all-organic coating can be deposited. Furthermore, combining the ALD with an MLD one can be used to produce a hybrid organic-inorganic coating. The process of a typical hybrid MLD coating of alucone (aluminum organic) is shown in Figure 15b. Rather than pulsing in water, ethylene glycol is introduced to form an inorganic-organic hybrid film.^[200] Though no references can be indexed about the application of MLD in cathode materials surface modifications, its versatile design will certainly find potential in this field. With the fast development of conductive polymer coatings using MLD,^[201] and the pyrolysis of a polymer coating into conductive carbon,^[202] it is rationally predicable that MLD will

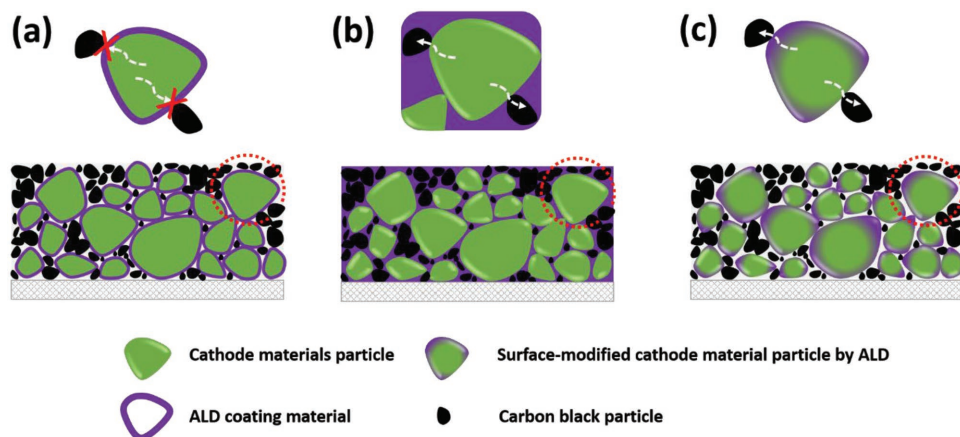


Figure 16. Schematic illustration of the difference between ALD coating on a) powders, b) directly on electrodes, and c) postannealed ALD coated cathode materials.

be a powerful technique targeting at cathode materials surface modifications.

4.4. Industrialization of ALD/MLD Techniques for LIB Applications

While there is a plentiful researches demonstrating the effectiveness of ALD techniques for cathode surface modifications, speculations arise when it comes to the large-scale deposition in practical applications. In the quest for the industrialization of ALD technique, spatial ALD (SALD) has been developed by a couple of companies.^[203] As illustrated in **Figure 17a,b**, the SALD is based on spatial separation instead of temporal (precursors are introduced pulse by pulse) separation. Compared to conventional ALD processes that fix the substrate and introduce the precursors one by one, SALD allows the substrate to move between different reaction chambers (Figure 17c). Each of the reaction chambers contains one type of precursor and is physically separated from other chambers, thus preventing intercontaminations. Such a design allows for continuous deposition without intermittent gas filling and purging. Also, there is no interruption caused by sample loading/unloading and system heating/cooling, making the whole process time-efficient.^[204] More importantly, in conventional ALD processes, the unreacted precursor is purged away by inert gas or deposited on the chamber wall when the other precursor is introduced, leading to a major loss of precursors. However, in the SALD technique, the precursor is not purged away, instead, it stays in the chamber and participates in the deposition half reaction whenever fresh substrate is moved into the chamber. Besides, with only one type of precursor in a given chamber, there is no loss due to deposition on the reaction chamber walls. These benefits of the SALD technique makes the industrialization of ALD/MLD technically and economically feasible.^[203] With respect to the application of SALD in LIBs, a roll-to-roll SALD configuration (Figure 17d) developed for flexible substrate works well for electrode coatings. In this setup, the precursors are kept in a drum with the substrate pulling over it. The thickness is dictated by the rotation speed of the drum and the speed at which the substrate moves.^[203,205]

In the case of deposition on powder samples in large scale, tremendous efforts have been made on designing economically

feasible and easy-to-operate reactors. Powdered cathode materials are less sensitive to the size of the reaction chamber, hence the most critical parameter that needs to be concerned is the uniformity of deposition. Regarding this, many reactor designs

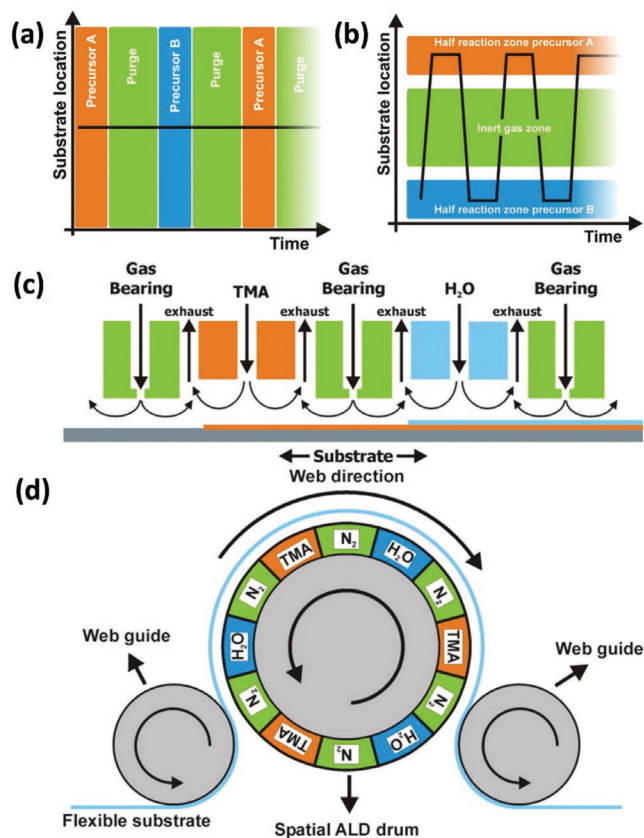


Figure 17. Schematic illustrations of a) a conventional ALD with the variation of time and position of the substrate (black line), and b) a spatial ALD with the variation of time and position of the substrate (black line). c) Principle of a close proximity spatial ALD reactor using the deposition of Al_2O_3 as an example. d) Roll-to-roll concept for ALD coating of flexible substrates using the deposition of Al_2O_3 as an example. Reproduced with permission.^[203] Copyright 2012, American Vacuum Society.

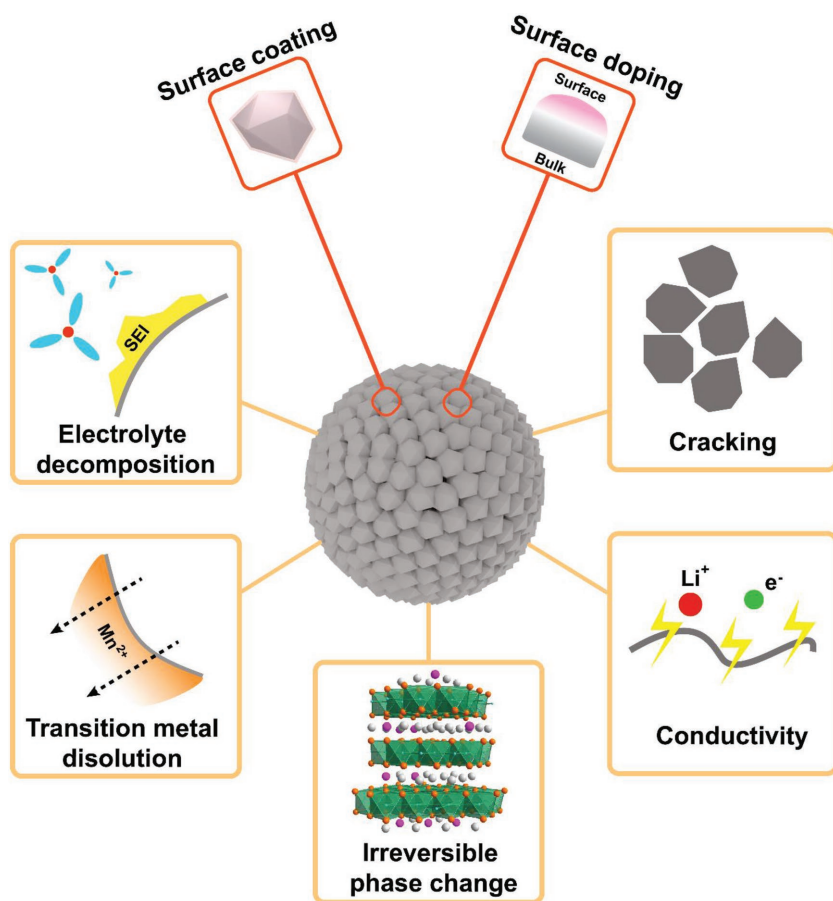


Figure 18. Schematic illustrations of the surface behaviors of cathode materials and modification methods.

such as fluidization in bed reactors, rotary reactors and centrifugally accelerated fluidization have been developed. These reactors fulfill the target of uniform coating by agitating the powder during deposition.^[206]

5. Conclusions and Outlook

5.1. Conclusions

We have covered surface and subsurface issues on cathode materials such as phase transition, mechanical cracking, electrolyte decomposition, transition metal dissolution, conductivity and air instability in this review (Figure 18). These surface and subsurface issues do not occur independently but work synergistically leading to material failure. Although a number of various surface modification strategies have been outlined, the question of an ideal modification technique still remains elusive. Undoubtedly, the surface modification method employed is dependent on the problem that is set out to be addressed. Simple coating might work moderately in suppressing metal dissolution, electrolyte decomposition and improving conductivity, but is of less use when the intrinsic phase change is the issue. The application of a rough, inconsistent coating will not

impede electronic or ionic conductivity badly but is insufficient in protecting against attack by acids generated in the electrolyte. Surface doping has been shown to mitigate surface phase transitions, improve the conductivity and decrease the metal dissolution. However, this technique is restricted by available elements and the control over doping amount is difficult. Moreover, the doping process is still not fully understood and requires further scientific investigation. Conformal coatings using ALD or MLD can protect the electrode effectively, but the dense nature of these coatings inhibits electron and lithium-ion diffusion and coating thickness plays a pivotal role. One method of overcoming the inherent denseness of ALD and MLD coatings is to deposit directly on the electrode but it also requires the use of a binder that can withstand high temperature processing. In addition to this, the electrochemical stability of the ALD/MLD-derived coating materials must be taken into consideration, in case of the loss of functionality.

5.2. Outlook

With these schemes in mind, we envisage that surface modification method should be developing in a way of integrating the advantages of these methods. For example, surface doping design with ALD modified cathode materials and direct fabrication of conformal conductive and electrochemically stable polymer coating via MLD. In a more sophisticated scenario, hybrid coatings that comprise of both good electrical and ionic conductivity would be very promising. These approaches are also highly dependent on the development of advanced coating materials derived from ALD/MLD, which is a major challenge due to the relative scarcity and high cost of precursors that can fit into the ALD/MLD chemistries.^[177,207] On the other hand, full utilization of advanced surface-sensitive characterization techniques such as HRTEM, STEM-HAADF, TOF-SIMS, AES, XPS, XANES, and so forth and the combination with in situ capability will undoubtedly promote a deeper understanding of surface behaviors of cathode materials. Thirdly, new redox chemistries, such as anionic redox reaction involved in Li-rich NMC systems and phase transition involved in high Ni-containing NMC cathode materials may induce unexpected surface issues, fundamental understandings on the origin, reaction routes and consequences are urgently needed, computational simulations have been proven effective in predicting the participation of oxygen, yet more efforts are to be devoted to better utilization of this mechanism.^[208] Fourth, recent advancement of LIBs pursues high energy density by utilizing lithium metal as the anode. Progress has been made by using high concentration electrolyte.^[67,209] However, there is very limited information regarding the cathode surface/subsurface reactions within

this particular combination, hence future direction should include detailed analysis of this topic. Overall, a proper design of surface coating that fulfills these criteria, together with solid evidence on how it works toward performance improvement, will undeniably lay milestones in the further development of high-power LIBs.

Acknowledgements

This research was supported by the Natural Science and Engineering Research Council of Canada (NSERC), the Canada Research Chair Program (CRC), the Canada Foundation for Innovation (CFI), and the University of Western Ontario (UWO).

Conflict of Interest

The authors declare no conflict of interest.

Keywords

cathode materials, lithium-ion batteries, surface modification

Received: July 4, 2018

Revised: July 26, 2018

Published online:

- [1] a) B. Scrosati, *Nature* **1995**, 373, 557; b) J.-M. Tarascon, M. Armand, *Nature* **2001**, 414, 359; c) J. B. Goodenough, Y. Kim, *Chem. Mater.* **2010**, 22, 587; d) J. B. Goodenough, *Acc. Chem. Res.* **2013**, 46, 1053; e) J.-H. Kim, N. P. W. Pieczonka, P. Lu, Z. Liu, R. Qiao, W. Yang, M. M. Tessema, Y.-K. Sun, B. R. Powell, *Adv. Mater. Interfaces* **2015**, 2, 1500109; f) Y. Zhao, Y. Ding, Y. Li, L. Peng, H. R. Byon, J. B. Goodenough, G. Yu, *Chem. Soc. Rev.* **2015**, 44, 7968.
- [2] A. Sakti, J. J. Michalek, E. R. H. Fuchs, J. F. Whitacre, *J. Power Sources* **2015**, 273, 966.
- [3] Y. Nishi, *Chem. Rec.* **2001**, 1, 406.
- [4] N. Nitta, F. X. Wu, J. T. Lee, G. Yushin, *Mater Today* **2015**, 18, 252.
- [5] J. Cabana, L. Monconduit, D. Larcher, M. R. Palacin, *Adv. Mater.* **2010**, 22, E170.
- [6] A. Kwade, W. Haselrieder, R. Leithoff, A. Modlinger, F. Dietrich, K. Droeder, *Nano Energy* **2018**, 3, 290.
- [7] R. Schmich, W. Ralf, G. Hörpel, T. Placke, M. Winter, *Nat. Energy* **2018**, 3, 267.
- [8] a) M. S. Whittingham, *Chem. Rev.* **2004**, 104, 4271; b) J. M. Tarascon, M. Armand, *Nature* **2001**, 414, 359; c) M. Armand, J. M. Tarascon, *Nature* **2008**, 451, 652; d) P. G. Bruce, B. Scrosati, J. M. Tarascon, *Angew. Chem.* **2008**, 47, 2930; e) M. R. Palacin, *Chem. Soc. Rev.* **2009**, 38, 2565; f) F. Xie, L. Zhang, D. Su, M. Jaroniec, S. Z. Qiao, *Adv. Mater.* **2017**, 29, 1700989; g) C. Zeng, F. Xie, X. Yang, M. Jaroniec, L. Zhang, S. Z. Qiao, *Angew. Chem.* **2018**, 57, 8540; h) C. Ye, L. Zhang, C. Guo, D. Li, A. Vasileff, H. Wang, S.-Z. Qiao, *Adv. Funct. Mater.* **2017**, 27, 1702524.
- [9] a) K. T. Lee, S. Jeong, J. Cho, *Acc. Chem. Res.* **2013**, 46, 1161; b) M. S. Islam, C. A. Fisher, *Chem. Soc. Rev.* **2014**, 43, 185.
- [10] T. Ohzuku, A. Ueda, M. Nagayama, Y. Iwakoshi, H. Komori, *Electrochim. Acta* **1993**, 38, 1159.
- [11] G. G. Amatucci, *J. Electrochem. Soc.* **1996**, 143, 1114.
- [12] Z. Chen, Z. Lu, J. R. Dahn, *J. Electrochem. Soc.* **2002**, 149, A1604.
- [13] E. Rossen, J. Reimers, J. Dahn, *Solid State Ionics* **1993**, 62, 53.
- [14] E. Antolini, *Solid State Ionics* **2004**, 170, 159.
- [15] S. Kang, *Solid State Ionics* **1999**, 120, 155.
- [16] Y. Shao-Horn, S. A. Hackney, A. J. Kahaian, M. M. Thackeray, *J. Solid State Chem.* **2002**, 168, 60.
- [17] a) H. Wang, *J. Electrochem. Soc.* **1999**, 146, 473; b) H. Gabrisch, R. Yazami, B. Fultz, *J. Power Sources* **2003**, 119–121, 674.
- [18] J.-H. Shim, K.-S. Lee, A. Missyul, J. Lee, B. Linn, E. C. Lee, S. Lee, *Chem. Mater.* **2015**, 27, 3273.
- [19] a) T. Ohzuku, *J. Electrochem. Soc.* **1993**, 140, 1862; b) A. R. Armstrong, N. Dupre, A. J. Paterson, C. P. Grey, P. G. Bruce, *Chem. Mater.* **2004**, 16, 3106; c) P. Kalyani, N. Kalaiselvi, *Sci. Technol. Adv. Mater.* **2005**, 6, 689.
- [20] W. Li, B. Song, A. Manthiram, *Chem. Soc. Rev.* **2017**, 46, 3006.
- [21] A. Rougier, C. Delmas, A. V. Chadwick, *Solid State Commun.* **1995**, 94, 123.
- [22] M. Arroyo y de Dompablo, C. Marianetti, A. Van der Ven, G. Ceder, *Phys. Rev. B* **2001**, 63, 144107.
- [23] a) J. Kim, B. H. Kim, Y. H. Baik, P. K. Chang, H. S. Park, K. Amine, *J. Power Sources* **2006**, 158, 641; b) R. Sathiyamoorthi, P. Shakkthivel, S. Ramalakshmi, Y.-G. Shul, *J. Power Sources* **2007**, 171, 922.
- [24] a) A. W. Moses, H. G. G. Flores, J.-G. Kim, M. A. Langell, *Appl. Surf. Sci.* **2007**, 253, 4782; b) J. M. Wang, J. P. Hu, C. Y. Ouyang, S. Q. Shi, M. S. Lei, *Solid State Commun.* **2011**, 151, 234.
- [25] a) S. Muto, Y. Sasano, K. Tatsumi, T. Sasaki, K. Horibuchi, Y. Takeuchi, Y. Ukyo, *J. Electrochem. Soc.* **2009**, 156, A371; b) R. Robert, C. Villevieille, P. Novák, *J. Mater. Chem. A* **2014**, 2, 8589; c) T. Nonaka, C. Okuda, Y. Seno, K. Koumoto, Y. Ukyo, *Ceram. Int.* **2008**, 34, 859; d) T. Nonaka, C. Okuda, Y. Seno, Y. Kondo, K. Koumoto, Y. Ukyo, *J. Electrochem. Soc.* **2007**, 154, A353.
- [26] F. Lin, I. M. Markus, D. Nordlund, T. C. Weng, M. D. Asta, H. L. Xin, M. M. Doeff, *Nat. Commun.* **2014**, 5, 3529.
- [27] P. Yan, J. Zheng, J. G. Zhang, C. Wang, *Nano Lett.* **2017**, 17, 3946.
- [28] S. K. Jung, H. Gwon, J. Hong, K. Y. Park, D. H. Seo, H. Kim, J. Hyun, W. Yang, K. Kang, *Adv. Energy Mater.* **2014**, 4.
- [29] a) Y. Bi, T. Wang, M. Liu, R. Du, W. Yang, Z. Liu, Z. Peng, Y. Liu, D. Wang, X. Sun, *RSC Adv.* **2016**, 6, 19233; b) S. Hwang, S. M. Kim, S.-M. Bak, K. Y. Chung, W. Chang, *Chem. Mater.* **2015**, 27, 6044.
- [30] P. F. Yan, J. M. Zheng, D. P. Lv, Y. Wei, J. X. Zheng, Z. G. Wang, S. Kuppam, J. G. Yu, L. L. Luo, D. Edwards, M. Olszta, K. Amine, J. Liu, J. Xiao, F. Pan, G. Y. Chen, J. G. Zhang, C. M. Wang, *Chem. Mater.* **2015**, 27, 5393.
- [31] a) B.-B. Lim, S.-J. Yoon, K.-J. Park, C. S. Yoon, S.-J. Kim, J. J. Lee, Y.-K. Sun, *Adv. Funct. Mater.* **2015**, 25, 4673; b) Y. K. Sun, Z. Chen, H. J. Noh, D. J. Lee, H. G. Jung, Y. Ren, S. Wang, C. S. Yoon, S. T. Myung, K. Amine, *Nat. Mater.* **2012**, 11, 942.
- [32] Y. K. Sun, S. T. Myung, B. C. Park, J. Prakash, I. Belharouak, K. Amine, *Nat. Mater.* **2009**, 8, 320.
- [33] D.-W. Jun, C. S. Yoon, U.-H. Kim, Y.-K. Sun, *Chem. Mater.* **2017**, 29, 5048.
- [34] P. K. Nayak, E. M. Erickson, F. Schipper, T. R. Penki, N. Munichandraiah, P. Adelhelm, H. Sclar, F. Amalraj, B. Markovsky, D. Aurbach, *Adv. Energy Mater.* **2018**, 8, 1702397.
- [35] a) Y. Shin, H. Ding, K. A. Persson, *Chem. Mater.* **2016**, 28, 2081; b) J. Zheng, S. Myeong, W. Cho, P. Yan, J. Xiao, C. Wang, J. Cho, J.-G. Zhang, *Adv. Energy Mater.* **2017**, 7, 1601284.
- [36] H. Yu, R. Ishikawa, Y. G. So, N. Shibata, T. Kudo, H. Zhou, Y. Ikuhara, *Angew. Chem.* **2013**, 52, 5969.
- [37] P. Yan, A. Nie, J. Zheng, Y. Zhou, D. Lu, X. Zhang, R. Xu, I. Belharouak, X. Zu, J. Xiao, K. Amine, J. Liu, F. Gao, R. Shahbazian-Yassar, J. G. Zhang, C. M. Wang, *Nano Lett.* **2015**, 15, 514.

- [38] K. A. Jarvis, Z. Deng, L. F. Allard, A. Manthiram, P. J. Ferreira, *Chem. Mater.* **2011**, *23*, 3614.
- [39] A. K. Shukla, Q. M. Ramasse, C. Ophus, H. Duncan, F. Hage, G. Chen, *Nat. Commun.* **2015**, *6*, 8711.
- [40] P. Yan, J. Zheng, J. Xiao, C.-M. Wang, J.-G. Zhang, *Front. Energy Res.* **2015**, *3*, 26.
- [41] a) J. Zheng, P. Xu, M. Gu, J. Xiao, N. D. Browning, P. Yan, C. Wang, J.-G. Zhang, *Chem. Mater.* **2015**, *27*, 1381; b) C.-G. Han, C. Zhu, G. Saito, T. Akiyama, *Electrochim. Acta* **2016**, *209*, 225; c) P. Yan, J. Zheng, J. Zheng, Z. Wang, G. Teng, S. Kuppan, J. Xiao, G. Chen, F. Pan, J.-G. Zhang, C.-M. Wang, *Adv. Energy Mater.* **2016**, *6*, 1502455.
- [42] P. Rozier, J. M. Tarascon, *J. Electrochem. Soc.* **2015**, *162*, A2490.
- [43] S. Kuppan, A. K. Shukla, D. Membreno, D. Nordlund, G. Chen, *Adv. Energy Mater.* **2017**, *7*, 1602010.
- [44] a) D. H. Seo, J. Lee, A. Urban, R. Malik, S. Kang, G. Ceder, *Nat. Chem.* **2016**, *8*, 692; b) S. Muhammad, H. Kim, Y. Kim, D. Kim, J. H. Song, J. Yoon, J.-H. Park, S.-J. Ahn, S.-H. Kang, M. M. Thackeray, W.-S. Yoon, *Nano Energy* **2016**, *21*, 172; c) K. Luo, M. R. Roberts, R. Hao, N. Guerrini, D. M. Pickup, Y. S. Liu, K. Edstrom, J. Guo, A. V. Chadwick, L. C. Duda, P. G. Bruce, *Nat. Chem.* **2016**, *8*, 684.
- [45] S. Hy, F. Felix, J. Rick, W. N. Su, B. J. Hwang, *J. Am. Chem. Soc.* **2014**, *136*, 999.
- [46] J. M. Tarascon, E. Wang, F. K. Shokoohi, W. R. Mckinnon, S. Colson, *J. Electrochem. Soc.* **1991**, *138*, 2859.
- [47] a) Y. Shao-Horn, S. A. Hackney, A. J. Kahaian, K. D. Kepler, E. Skinner, J. T. Vaughey, M. M. Thackeray, *J. Power Sources* **1999**, *81–82*, 496; b) M. M. Thackeray, *Electrochem. Solid-State Lett.* **1999**, *1*, 7; c) K. Y. Chung, K. B. Kim, *J. Electrochem. Soc.* **2002**, *149*, A79.
- [48] K. Y. Chung, W.-S. Yoon, H. S. Lee, X.-Q. Yang, J. McBreen, B. H. Deng, X. Q. Wang, M. Yoshio, R. Wang, J. Gui, M. Okada, *J. Power Sources* **2005**, *146*, 226.
- [49] K. Y. Chung, W. S. Yoon, K. B. Kim, X. Q. Yang, S. M. Oh, *J. Electrochem. Soc.* **2004**, *151*, A484.
- [50] T. Eriksson, T. Gustafsson, J. O. Thomas, *Electrochem. Solid-State Lett.* **2002**, *5*, A35.
- [51] R. Alcántara, M. Jaraba, P. Lavela, J. L. Tirado, P. Biensan, A. de Guibert, C. Jordy, J. P. Peres, *Chem. Mater.* **2003**, *15*, 2376.
- [52] a) K. Y. Chung, W.-S. Yoon, K.-B. Kim, X.-Q. Yang, S. M. Oh, *J. Electrochem. Soc.* **2004**, *151*, A484; b) J.-H. Kim, N. P. W. Pieczonka, Z. Li, Y. Wu, S. Harris, B. R. Powell, *Electrochim. Acta* **2013**, *90*, 556; c) P. V. Sushko, K. M. Rosso, J.-G. Zhang, J. Liu, M. L. Sushko, *Adv. Funct. Mater.* **2013**, *23*, 5530.
- [53] a) R. Deshpande, Y. Qi, Y.-T. Cheng, *J. Electrochem. Soc.* **2010**, *157*, A967; b) R. Deshpande, Y.-T. Cheng, M. W. Verbrugge, *J. Power Sources* **2010**, *195*, 5081.
- [54] a) K. Zhao, M. Pharr, J. J. Vlassak, Z. Suo, *J. Appl. Phys.* **2010**, *108*, 073517; b) W. H. Woodford, Y.-M. Chiang, W. C. Carter, *J. Electrochem. Soc.* **2010**, *157*, A1052.
- [55] A. Ito, D. Li, Y. Sato, M. Arao, M. Watanabe, M. Hatano, H. Horie, Y. Ohsawa, *J. Power Sources* **2010**, *195*, 567.
- [56] P. Yan, J. Zheng, M. Gu, J. Xiao, J. G. Zhang, C. M. Wang, *Nat. Commun.* **2017**, *8*, 14101.
- [57] P. Yan, J. Zheng, T. Chen, L. Luo, Y. Jiang, K. Wang, M. Sui, J.-G. Zhang, S. Zhang, C. Wang, *Nat. Commun.* **2018**, *9*, 2437.
- [58] J. Zheng, M. Gu, J. Xiao, P. Zuo, C. Wang, J. G. Zhang, *Nano Lett.* **2013**, *13*, 3824.
- [59] M. Singh, J. Kaiser, H. Hahn, *J. Electrochem. Soc.* **2015**, *162*, A1196.
- [60] D. J. Miller, C. Proff, J. G. Wen, D. P. Abraham, J. Bareño, *Adv. Energy Mater.* **2013**, *3*, 1098.
- [61] K. Xu, *Chem. Rev.* **2004**, *104*, 4303.
- [62] V. Aravindan, J. Gnanaraj, S. Madhavi, H. K. Liu, *Chemistry* **2011**, *17*, 14326.
- [63] a) X. R. Zhang, R. Kostecki, T. J. Richardson, J. K. Pugh, P. N. Ross, *J. Electrochem. Soc.* **2001**, *148*, A1341; b) M. Egashira, H. Takahashi, S. Okada, J. Yamaki, *J. Power Sources* **2001**, *92*, 267.
- [64] S. Shi, P. Lu, Z. Liu, Y. Qi, L. G. Hector Jr., H. Li, S. J. Harris, *J. Am. Chem. Soc.* **2012**, *134*, 15476.
- [65] M. Winter, *Z. Phys. Chem.* **2009**, *223*, 1395.
- [66] D. Aurbach, B. Markovsky, G. Salitra, E. Markevich, Y. Talyosoff, M. Koltypin, L. Nazar, B. Ellis, D. Kovacheva, *J. Power Sources* **2007**, *165*, 491.
- [67] S. Chen, J. Zheng, D. Mei, K. S. Han, M. H. Engelhard, W. Zhao, W. Xu, J. Liu, J. G. Zhang, *Adv. Mater.* **2018**, *30*, e1706102.
- [68] a) P. Lu, S. J. Harris, *Electrochem. Commun.* **2011**, *13*, 1035; b) P. Verma, P. Maire, P. Novák, *Electrochim. Acta* **2010**, *55*, 6332.
- [69] Z. Zhang, L. Hu, H. Wu, W. Weng, M. Koh, P. C. Redfern, L. A. Curtiss, K. Amine, *Energy Environ. Sci.* **2013**, *6*, 1806.
- [70] J. B. Goodenough, Y. Kim, *J. Power Sources* **2011**, *196*, 6688.
- [71] a) D. D. MacNeil, J. R. Dahn, *J. Electrochem. Soc.* **2003**, *150*, A21; b) M. Gauthier, T. J. Carney, A. Grimaud, L. Giordano, N. Pour, H. H. Chang, D. P. Fenning, S. F. Lux, O. Paschos, C. Bauer, F. Maglia, S. Lupart, P. Lamp, Y. Shao-Horn, *J. Phys. Chem. Lett.* **2015**, *6*, 4653.
- [72] S. S. Zhang, *J. Power Sources* **2006**, *162*, 1379.
- [73] J.-G. Han, J. B. Lee, A. Cha, T. K. Lee, W. Cho, S. Chae, S. J. Kang, S. K. Kwak, J. Cho, S. Y. Hong, N.-S. Choi, *Energy Environ. Sci.* **2018**, *11*, 1552.
- [74] a) D. Aurbach, *J. Power Sources* **2000**, *89*, 206; b) U. Heider, R. Oesten, M. Jungnitz, *J. Power Sources* **1999**, *81–82*, 119.
- [75] T. Kawamura, S. Okada, J.-i. Yamaki, *J. Power Sources* **2006**, *156*, 547.
- [76] X. Li, J. Liu, M. N. Banis, A. Lushington, R. Li, M. Cai, X. Sun, *Energy Environ. Sci.* **2014**, *7*, 768.
- [77] a) W. Choi, A. Manthiram, *J. Electrochem. Soc.* **2006**, *153*, A1760; b) D. H. Jang, *J. Electrochem. Soc.* **1996**, *143*, 2204.
- [78] a) T. Aoshima, K. Okahara, C. Kiyohara, K. Shizuka, *J. Power Sources* **2001**, *97–98*, 377; b) D. Kim, S. Park, O. B. Chae, J. H. Ryu, Y. U. Kim, R. Z. Yin, S. M. Oh, *J. Electrochem. Soc.* **2012**, *159*, A193.
- [79] C. Zhan, J. Lu, A. Jeremy Kropf, T. Wu, A. N. Jansen, Y. K. Sun, X. Qiu, K. Amine, *Nat. Commun.* **2013**, *4*, 2437.
- [80] C. Zhan, T. Wu, J. Lu, K. Amine, *Energy Environ. Sci.* **2018**, *11*, 243.
- [81] M. Hirayama, H. Ido, K. Kim, W. Cho, K. Tamura, J. Mizuki, R. Kanno, *J. Am. Chem. Soc.* **2010**, *132*, 15268.
- [82] N. P. W. Pieczonka, Z. Y. Liu, P. Lu, K. L. Olson, J. Moote, B. R. Powell, J. H. Kim, *J. Phys. Chem. C* **2013**, *117*, 15947.
- [83] W. Li, X. Liu, H. Celio, P. Smith, A. Dolocan, M. Chi, A. Manthiram, *Adv. Energy Mater.* **2018**, *8*.
- [84] a) S.-T. Myung, F. Maglia, K.-J. Park, C. S. Yoon, P. Lamp, S.-J. Kim, Y.-K. Sun, *ACS Energy Lett.* **2017**, *2*, 196; b) H. S. Liu, Z. R. Zhang, Z. L. Gong, Y. Yang, *Electrochem. Solid-State Lett.* **2004**, *7*, A190.
- [85] B. Xiao, B. Wang, J. Liu, K. Kaliyappan, Q. Sun, Y. Liu, G. Dadheech, M. P. Balogh, L. Yang, T.-K. Sham, R. Li, M. Cai, X. Sun, *Nano Energy* **2017**, *34*, 120.
- [86] S. E. Renfrew, B. D. McCloskey, *J. Am. Chem. Soc.* **2017**, *139*, 17853.
- [87] Y. Bi, T. Wang, M. Liu, R. Du, W. Yang, Z. Liu, Z. Peng, Y. Liu, D. Wang, X. Sun, *RSC Adv.* **2016**, *6*, 19233.
- [88] A. Manthiram, J. C. Knight, S.-T. Myung, S.-M. Oh, Y.-K. Sun, *Adv. Energy Mater.* **2015**, *6*, 1501010.
- [89] a) J. Cho, *Electrochem. Solid-State Lett.* **1999**, *3*, 362; b) J. Cho, Y. J. Kim, B. Park, *Chem. Mater.* **2000**, *12*, 3788; c) J. Cho, Y. J. Kim, T.-J. Kim, B. Park, *Angew. Chem., Int. Ed.* **2001**, *40*, 3367; d) J. Cho, Y. J. Kim, B. Park, *J. Electrochem. Soc.* **2001**, *148*, A1110.
- [90] Z. Chen, J. R. Dahn, *Electrochem. Solid-State Lett.* **2002**, *5*, A213.
- [91] Z. Chen, J. R. Dahn, *Electrochem. Solid-State Lett.* **2003**, *6*, A221.
- [92] J.-H. Shim, S. Lee, S. S. Park, *Chem. Mater.* **2014**, *26*, 2537.
- [93] Y. Cho, P. Oh, J. Cho, *Nano Lett.* **2013**, *13*, 1145.

- [94] Y. Zhao, J. Li, J. R. Dahn, *Chem. Mater.* **2017**, *29*, 5239.
- [95] J. Lu, C. Zhan, T. Wu, J. Wen, Y. Lei, A. J. Kropf, H. Wu, D. J. Miller, J. W. Elam, Y. K. Sun, X. Qiu, K. Amine, *Nat. Commun.* **2014**, *5*, 5693.
- [96] B. Xiao, H. Liu, J. Liu, Q. Sun, B. Wang, K. Kaliyappan, Y. Zhao, M. N. Banis, Y. Liu, R. Li, T. K. Sham, G. A. Botton, M. Cai, X. Sun, *Adv. Mater.* **2017**.
- [97] R. J. Gummow, A. de Kock, M. M. Thackeray, *Solid State Ionics* **1994**, *69*, 59.
- [98] K. Y. Chung, C.-W. Ryu, K.-B. Kim, *J. Electrochem. Soc.* **2005**, *152*, A791.
- [99] L. Xiong, Y. Xu, T. Tao, X. Du, J. Li, *J. Mater. Chem.* **2011**, *21*, 4937.
- [100] M.-S. Park, J.-W. Lee, W. Choi, D. Im, S.-G. Doo, K.-S. Park, *J. Mater. Chem.* **2010**, *20*, 7208.
- [101] W. Liu, P. Oh, X. Liu, S. Myeong, W. Cho, J. Cho, *Adv. Energy Mater.* **2015**, *5*, 1500274.
- [102] R.-P. Qing, J.-L. Shi, D.-D. Xiao, X.-D. Zhang, Y.-X. Yin, Y.-B. Zhai, L. Gu, Y.-G. Guo, *Adv. Energy Mater.* **2015**, *5*, 1501914.
- [103] F. Wu, N. Li, Y. Su, H. Lu, L. Zhang, R. An, Z. Wang, L. Bao, S. Chen, *J. Mater. Chem.* **2012**, *22*, 1489.
- [104] Y. K. Sun, M. J. Lee, C. S. Yoon, J. Hassoun, K. Amine, B. Scrosati, *Adv. Mater.* **2012**, *24*, 1192.
- [105] J. R. Croy, M. Balasubramanian, D. Kim, S.-H. Kang, M. M. Thackeray, *Chem. Mater.* **2011**, *23*, 5415.
- [106] S.-H. Kang, M. M. Thackeray, *Electrochem. Commun.* **2009**, *11*, 748.
- [107] a) G. Xu, J. Li, Q. Xue, X. Ren, G. Yan, X. Wang, F. Kang, *J. Power Sources* **2014**, *248*, 894; b) H. Z. Zhang, Q. Q. Qiao, G. R. Li, S. H. Ye, X. P. Gao, *J. Mater. Chem.* **2012**, *22*, 13104; c) P. Yan, L. Xiao, J. Zheng, Y. Zhou, Y. He, X. Zu, S. X. Mao, J. Xiao, F. Gao, J.-G. Zhang, C.-M. Wang, *Chem. Mater.* **2015**, *27*, 975; d) J. Zhang, Z. Lei, J. Wang, Y. NuLi, J. Yang, *ACS Appl. Mater. Interfaces* **2015**, *7*, 15821.
- [108] B. Qiu, M. Zhang, L. Wu, J. Wang, Y. Xia, D. Qian, H. Liu, S. Hy, Y. Chen, K. An, Y. Zhu, Z. Liu, Y. S. Meng, *Nat. Commun.* **2016**, *7*, 12108.
- [109] C. S. Johnson, N. Li, J. T. Vaughey, S. A. Hackney, M. M. Thackeray, *Electrochem. Commun.* **2005**, *7*, 528.
- [110] Q. Xia, X. Zhao, M. Xu, Z. Ding, J. Liu, L. Chen, D. G. Ivey, W. Wei, *J. Mater. Chem. A* **2015**, *3*, 3995.
- [111] J. Zhao, R. Huang, W. Gao, J.-M. Zuo, X. F. Zhang, S. T. Misture, Y. Chen, J. V. Lockard, B. Zhang, S. Guo, M. R. Khoshi, K. Dooley, H. He, Y. Wang, *Adv. Energy Mater.* **2015**, *5*, 1401937.
- [112] L. Guo, N. Zhao, J. Li, C. He, C. Shi, E. Liu, *ACS Appl. Mater. Interfaces* **2015**, *7*, 391.
- [113] J. Zheng, M. Gu, J. Xiao, B. J. Polzin, P. Yan, X. Chen, C. Wang, J.-G. Zhang, *Chem. Mater.* **2014**, *26*, 6320.
- [114] S. Zhang, H. Gu, H. Pan, S. Yang, W. Du, X. Li, M. Gao, Y. Liu, M. Zhu, L. Ouyang, D. Jian, F. Pan, *Adv. Energy Mater.* **2017**, *7*, 1601066.
- [115] I. Bloom, L. Trahey, A. Abouimrane, I. Belharouak, X. Zhang, Q. Wu, W. Lu, D. P. Abraham, M. Bettge, J. W. Elam, X. Meng, A. K. Burrell, C. Ban, R. Tenent, J. Nanda, N. Dudney, *J. Power Sources* **2014**, *249*, 509.
- [116] P. Yan, J. Zheng, X. Zhang, R. Xu, K. Amine, J. Xiao, J.-G. Zhang, C.-M. Wang, *Chem. Mater.* **2016**, *28*, 857.
- [117] P. Yan, J. Zheng, J. Liu, B. Wang, X. Cheng, Y. Zhang, X. Sun, C. Wang, J.-G. Zhang, *Nat. Energy* **2018**, *3*, 600.
- [118] a) K. Araki, N. Taguchi, H. Sakaebe, K. Tatsumi, Z. Ogumi, *J. Power Sources* **2014**, *269*, 236; b) S.-H. Lee, C. S. Yoon, K. Amine, Y.-K. Sun, *J. Power Sources* **2013**, *234*, 201; c) Y. Kim, G. M. Veith, J. Nanda, R. R. Unocic, M. Chi, N. J. Dudney, *Electrochim. Acta* **2011**, *56*, 6573.
- [119] Y. Yang, X.-Z. Liao, Z.-F. Ma, B.-F. Wang, L. He, Y.-S. He, *Electrochem. Commun.* **2009**, *11*, 1277.
- [120] C. Wang, H. Wu, Z. Chen, M. T. McDowell, Y. Cui, Z. Bao, *Nat. Chem.* **2013**, *5*, 1042.
- [121] X. Li, A. Lushington, J. Liu, R. Li, X. Sun, *Chem. Commun.* **2014**, *50*, 9757.
- [122] a) R. Guo, P. Shi, X. Cheng, L. Sun, *Electrochim. Acta* **2009**, *54*, 5796; b) Z. Wang, C. Wu, L. Liu, F. Wu, L. Chen, X. Huang, *J. Electrochem. Soc.* **2002**, *149*, A466; c) K. W. Kim, S.-W. Lee, K.-S. Han, H. J. Chung, S. I. Woo, *Electrochim. Acta* **2003**, *48*, 4223; d) J. S. Kim, C. S. Johnson, J. T. Vaughey, S. A. Hackney, K. A. Walz, W. A. Zeltner, M. A. Anderson, M. M. Thackeray, *J. Electrochem. Soc.* **2004**, *151*, A1755; e) Y. K. Sun, K. J. Hong, J. Prakash, K. Amine, *Electrochem. Commun.* **2002**, *4*, 344; f) Z. R. Zhang, H. S. Liu, Z. L. Gong, Y. Yang, *J. Power Sources* **2004**, *129*, 101; g) S. B. Park, H. C. Shin, W.-G. Lee, W. I. Cho, H. Jang, *J. Power Sources* **2008**, *180*, 597.
- [123] Y. K. Sun, S. W. Cho, S. T. Myung, K. Amine, J. Prakash, *Electrochim. Acta* **2007**, *53*, 1013.
- [124] a) K. Yang, L.-Z. Fan, J. Guo, X. Qu, *Electrochim. Acta* **2012**, *63*, 363; b) Z. Yang, Q. Qiao, W. Yang, *Electrochim. Acta* **2011**, *56*, 4791; c) K.-S. Lee, S.-T. Myung, D.-W. Kim, Y.-K. Sun, *J. Power Sources* **2011**, *196*, 6974; d) J. M. Zheng, Z. R. Zhang, X. B. Wu, Z. X. Dong, Z. Zhu, Y. Yang, *J. Electrochem. Soc.* **2008**, *155*, A775.
- [125] a) J. Zhou, D. Hong, J. Wang, Y. Hu, X. Xie, H. Fang, *Phys. Chem. Chem. Phys.* **2014**, *16*, 13838; b) R. Kurian, K. Kunnus, P. Wernet, S. M. Butorin, P. Glatzel, F. M. de Groot, *J. Phys.: Condens. Matter* **2012**, *24*, 452201.
- [126] Z. Wu, S. Ji, J. Zheng, Z. Hu, S. Xiao, Y. Wei, Z. Zhuo, Y. Lin, W. Yang, K. Xu, K. Amine, F. Pan, *Nano Lett.* **2015**, *15*, 5590.
- [127] B. Xiao, J. Liu, Q. Sun, B. Wang, M. N. Banis, D. Zhao, Z. Wang, R. Li, X. Cui, T.-K. Sham, X. Sun, *Adv. Sci.* **2015**, *2*, 1500022.
- [128] G. Alva, C. Kim, T. Yi, J. B. Cook, L. Xu, G. M. Nolis, J. Cabana, *J. Phys. Chem. C* **2014**, *118*, 10596.
- [129] L. Dahéron, R. Dedryvère, H. Martinez, D. Flahaut, M. Ménétrier, C. Delmas, D. Gonbeau, *Chem. Mater.* **2009**, *21*, 5607.
- [130] a) A. Eftekhari, *J. Power Sources* **2004**, *130*, 260; b) J. T. Son, K. S. Park, H. G. Kim, H. T. Chung, *J. Power Sources* **2004**, *126*, 182.
- [131] a) C. Liu, J. An, R. Guo, Y. Li, L. Liu, *J. Alloys Compd.* **2013**, *563*, 33; b) Y. S. Hu, Y. G. Guo, R. Dominko, M. Gaberscek, J. Jamnik, J. Maier, *Adv. Mater.* **2007**, *19*, 1963.
- [132] Y. Q. Wang, L. Gu, Y. G. Guo, H. Li, X. Q. He, S. Tsukimoto, Y. Ikuhara, L. J. Wan, *J. Am. Chem. Soc.* **2012**, *134*, 7874.
- [133] a) Y.-H. Huang, K.-S. Park, J. B. Goodenough, *J. Electrochem. Soc.* **2006**, *153*, A2282; b) Y.-H. Huang, J. B. Goodenough, *Chem. Mater.* **2008**, *20*, 7237; c) A. Vadivel Murugan, T. Muraliganth, A. Manthiram, *Electrochem. Commun.* **2008**, *10*, 903; d) M. C. Kim, S. H. Kim, V. Aravindan, W. S. Kim, S. Y. Lee, Y. S. Lee, *J. Electrochem. Soc.* **2013**, *160*, A1003; e) Y.-m. Bai, P. Qiu, Z.-I. Wen, S.-c. Han, *J. Alloys Compd.* **2010**, *508*, 1.
- [134] a) J. Yang, J. Wang, Y. Tang, D. Wang, X. Li, Y. Hu, R. Li, G. Liang, T.-K. Sham, X. Sun, *Energy Environ. Sci.* **2013**, *6*, 1521; b) J. Yang, J. Wang, D. Wang, X. Li, D. Geng, G. Liang, M. Gauthier, R. Li, X. Sun, *J. Power Sources* **2012**, *208*, 340; c) J. Yang, J. Wang, X. Li, D. Wang, J. Liu, G. Liang, M. Gauthier, Y. Li, D. Geng, R. Li, X. Sun, *J. Mater. Chem.* **2012**, *22*, 7537; d) J. Yang, J. Wang, Y. Tang, D. Wang, B. Xiao, X. Li, R. Li, G. Liang, T.-K. Sham, X. Sun, *J. Mater. Chem. A* **2013**, *1*, 7306.
- [135] H. K. Noh, H. S. Park, H. Y. Jeong, S. U. Lee, H. K. Song, *Angew. Chem.* **2014**, *53*, 5059.
- [136] H. Liu, C. Chen, C. Du, X. He, G. Yin, B. Song, P. Zuo, X. Cheng, Y. Ma, Y. Gao, *J. Mater. Chem. A* **2015**, *3*, 2634.
- [137] X. Miao, H. Ni, H. Zhang, C. Wang, J. Fang, G. Yang, *J. Power Sources* **2014**, *264*, 147.
- [138] a) W. Choi, A. Benayard, J.-H. Park, J. Park, S.-G. Doo, J. Mun, *Electrochim. Acta* **2014**, *117*, 492; b) Y. Kim, N. J. Dudney, M. Chi, S. K. Martha, J. Nanda, G. M. Veith, C. Liang, *J. Electrochem. Soc.*

- 2013, 160, A3113; c) H. G. Song, K.-S. Park, Y. J. Park, *Solid State Ionics* **2012**, 225, 532; d) H. G. Song, J. Y. Kim, K. T. Kim, Y. J. Park, *J. Power Sources* **2011**, 196, 6847; e) A. Sakuda, A. Hayashi, M. Tatsumisago, *J. Power Sources* **2010**, 195, 599.
- [139] F. Cheng, Y. Xin, Y. Huang, J. Chen, H. Zhou, X. Zhang, *J. Power Sources* **2013**, 239, 181.
- [140] J.-M. Chen, Y.-D. Cho, C.-L. Hsiao, G. T.-K. Fey, *J. Power Sources* **2009**, 189, 279.
- [141] J. Chong, S. Xun, J. Zhang, X. Song, H. Xie, V. Battaglia, R. Wang, *Chemistry* **2014**, 20, 7479.
- [142] B. Wang, J. Liu, M. Norouzi Banis, Q. Sun, Y. Zhao, R. Li, T. K. Sham, X. Sun, *ACS Appl. Mater. Interfaces* **2017**, 9, 31786.
- [143] J. Wang, X. Sun, *Energy Environ. Sci.* **2012**, 5, 5163.
- [144] a) Y. Gao, *Solid State Ionics* **1996**, 84, 33; b) G. G. Amatucci, N. Pereira, T. Zheng, J. M. Tarascon, *J. Electrochem. Soc.* **2001**, 148, A171; c) S. J. Shi, J. P. Tu, Y. J. Mai, Y. Q. Zhang, C. D. Gu, X. L. Wang, *Electrochim. Acta* **2012**, 63, 112; d) S. Lee, Y. Cho, H. K. Song, K. T. Lee, J. Cho, *Angew. Chem.* **2012**, 51, 8748; e) J. Liu, Q. Wang, B. Reeja-Jayan, A. Manthiram, *Electrochem. Commun.* **2010**, 12, 750.
- [145] J. Liu, A. Manthiram, *Chem. Mater.* **2009**, 21, 1695.
- [146] Y. Huang, J. Chen, J. Ni, H. Zhou, X. Zhang, *J. Power Sources* **2009**, 188, 538.
- [147] A. T. Appapillai, A. N. Mansour, J. Cho, Y. Shao-Horn, *Chem. Mater.* **2007**, 19, 5748.
- [148] H. X. Dang, Y.-M. Lin, K. C. Klavetter, T. H. Cell, A. Heller, C. B. Mullins, *ChemElectroChem* **2014**, 1, 158.
- [149] M. Wilkening, V. Epp, A. Feldhoff, P. Heitjans, *J. Phys. Chem. C* **2008**, 112, 9291.
- [150] J. Janek, M. Martin, K. D. Becker, *Phys. Chem. Chem. Phys.* **2009**, 11, 3010.
- [151] M. Aykol, S. Kirklin, C. Wolverton, *Adv. Energy Mater.* **2014**, 4, 1400690.
- [152] a) J. Kim, H. Lee, H. Cha, M. Yoon, M. Park, J. Cho, *Adv. Energy Mater.* **2018**, 8, 1702028; b) C. S. Yoon, K.-J. Park, U.-H. Kim, K. H. Kang, H.-H. Ryu, Y.-K. Sun, *Chem. Mater.* **2017**, 29, 10436.
- [153] P. Oh, B. Song, W. Li, A. Manthiram, *J. Mater. Chem. A* **2016**, 4, 5839.
- [154] S. Chen, T. He, Y. Su, Y. Lu, L. Bao, L. Chen, Q. Zhang, J. Wang, R. Chen, F. Wu, *ACS Appl. Mater. Interfaces* **2017**, 9, 29732.
- [155] S. Kalluri, M. Yoon, M. Jo, S. Park, S. Myeong, J. Kim, S. X. Dou, Z. Guo, J. Cho, *Adv. Energy Mater.* **2017**, 7, 1601507.
- [156] A. Mauger, C. Julien, *Ionics* **2014**, 20, 751.
- [157] H. Cao, B. Xia, Y. Zhang, N. Xu, *Solid State Ionics* **2005**, 176, 911.
- [158] G. Li, Z. Yang, W. Yang, *J. Power Sources* **2008**, 183, 741.
- [159] J. H. Park, J. M. Kim, C. K. Lee, S. Y. Lee, *J. Power Sources* **2014**, 263, 209.
- [160] Y. Sun, J. Han, S. Myung, S. Lee, K. Amine, *Electrochem. Commun.* **2006**, 8, 821.
- [161] Y. Liu, S. Liu, Y. Wang, L. Chen, X. Chen, *J. Power Sources* **2013**, 222, 455.
- [162] a) Q.-Q. Qiao, G.-R. Li, Y.-L. Wang, X.-P. Gao, *J. Mater. Chem. A* **2016**, 4, 4440; b) S. Li, X. Fu, J. Zhou, Y. Han, P. Qi, X. Gao, X. Feng, B. Wang, *J. Mater. Chem. A* **2016**, 4, 5823.
- [163] a) K. Park, B. S. Lee, J. H. Park, S. G. Hong, *Phys. Chem. Chem. Phys.* **2016**, 18, 15861; b) H. Liu, D. Qian, M. G. Verde, M. Zhang, L. Baggetto, K. An, Y. Chen, K. J. Carroll, D. Lau, M. Chi, G. M. Veith, Y. S. Meng, *ACS Appl. Mater. Interfaces* **2015**, 7, 19189.
- [164] J. Liu, A. Manthiram, *J. Mater. Chem.* **2010**, 20, 3961.
- [165] Y. Chen, K. Xie, C. Zheng, Z. Ma, Z. Chen, *ACS Adv. Mater. Interfaces* **2014**, 6, 16888.
- [166] W.-K. Shin, Y.-S. Lee, D.-W. Kim, *J. Mater. Chem. A* **2014**, 2, 6863.
- [167] J.-H. Cho, J.-H. Park, M.-H. Lee, H.-K. Song, S.-Y. Lee, *Energy Environ. Sci.* **2012**, 5, 7124.
- [168] H.-B. Kang, S.-T. Myung, K. Amine, S.-M. Lee, Y.-K. Sun, *J. Power Sources* **2010**, 195, 2023.
- [169] L. Jaber-Ansari, K. P. Puntambekar, S. Kim, M. Aykol, L. Luo, J. Wu, B. D. Myers, H. Iddir, J. T. Russell, S. J. Saldaña, R. Kumar, M. M. Thackeray, L. A. Curtiss, V. P. Dravid, C. Wolverton, M. C. Hersam, *Adv. Energy Mater.* **2015**, 5, 1500646.
- [170] S. Zhao, Y. Bai, Q. Chang, Y. Yang, W. Zhang, *Electrochim. Acta* **2013**, 108, 727.
- [171] C. Qing, Y. Bai, J. Yang, W. Zhang, *Electrochim. Acta* **2011**, 56, 6612.
- [172] K. H. Jung, H.-G. Kim, Y. J. Park, *J. Alloys Compd.* **2011**, 509, 4426.
- [173] H. Ming, Y. R. Yan, J. Ming, J. Adkins, X. W. Li, Q. Zhou, J. W. Zheng, *Electrochim. Acta* **2014**, 120, 390.
- [174] a) M. D. Groner, J. W. Elam, F. H. Fabreguette, S. M. George, *Thin Solid Films* **2002**, 413, 186; b) J. W. Elam, M. D. Groner, S. M. George, *Rev. Sci. Instrum.* **2002**, 73, 2981; c) A. W. Ott, J. W. Klaus, J. M. Johnson, S. M. George, *Thin Solid Films* **1997**, 292, 135; d) A. C. Dillon, A. W. Ott, J. D. Way, S. M. George, *Surf. Sci.* **1995**, 322, 230; e) J.-F. Fan, K. Sugioka, K. Toyoda, *Jpn. J. Appl. Phys.* **1991**, 30, L1139.
- [175] a) J. W. Elam, N. P. Dasgupta, F. B. Prinz, *MRS Bull.* **2011**, 36, 899; b) C. Marichy, M. Bechelany, N. Pinna, *Adv. Mater.* **2012**, 24, 1017.
- [176] J. Liu, X. Sun, *Nanotechnology* **2015**, 26, 024001.
- [177] X. Meng, X. Q. Yang, X. Sun, *Adv. Mater.* **2012**, 24, 3589.
- [178] a) V. Miikkulainen, A. Ruud, E. Østregren, O. Nilsen, M. Laitinen, T. Sajavaara, H. Fjellvåg, *J. Phys. Chem. C* **2014**, 118, 1258; b) J. Liu, M. N. Banis, Q. Sun, A. Lushington, R. Li, T. K. Sham, X. Sun, *Adv. Mater.* **2014**, 26, 6472.
- [179] Y. S. Jung, A. S. Cavanagh, L. A. Riley, S. H. Kang, A. C. Dillon, M. D. Groner, S. M. George, S. H. Lee, *Adv. Mater.* **2010**, 22, 2172.
- [180] Y. S. Jung, A. S. Cavanagh, A. C. Dillon, M. D. Groner, S. M. George, S.-H. Lee, *J. Electrochem. Soc.* **2010**, 157, A75.
- [181] J.-T. Lee, F.-M. Wang, C.-S. Cheng, C.-C. Li, C.-H. Lin, *Electrochim. Acta* **2010**, 55, 4002.
- [182] I. D. Scott, Y. S. Jung, A. S. Cavanagh, Y. Yan, A. C. Dillon, S. M. George, S. H. Lee, *Nano Lett.* **2011**, 11, 414.
- [183] H.-M. Cheng, F.-M. Wang, J. P. Chu, R. Santhanam, J. Rick, S.-C. Lo, *J. Phys. Chem. C* **2012**, 116, 7629.
- [184] J. H. Woo, J. E. Trevey, A. S. Cavanagh, Y. S. Choi, S. C. Kim, S. M. George, K. H. Oh, S. H. Lee, *J. Electrochem. Soc.* **2012**, 159, A1120.
- [185] a) D. Guan, J. A. Jeevarajan, Y. Wang, *Nanoscale* **2011**, 3, 1465; b) D. Guan, Y. Wang, *Ionics* **2012**, 19, 1.
- [186] L. A. Riley, S. Van Atta, A. S. Cavanagh, Y. Yan, S. M. George, P. Liu, A. C. Dillon, S.-H. Lee, *J. Power Sources* **2011**, 196, 3317.
- [187] Y. Seok Jung, A. S. Cavanagh, Y. Yan, S. M. George, A. Manthiram, *J. Electrochem. Soc.* **2011**, 158, A1298.
- [188] X. Fang, F. Lin, D. Nordlund, M. Mecklenburg, M. Ge, J. Rong, A. Zhang, C. Shen, Y. Liu, Y. Cao, M. M. Doeff, C. Zhou, *Adv. Funct. Mater.* **2017**, 27, 1602873.
- [189] a) J. Zhao, Y. Wang, *Nano Energy* **2013**, 2, 882; b) J. Zhao, G. Qu, J. C. Flake, Y. Wang, *Chem. Commun.* **2012**, 48, 8108.
- [190] J. Zhao, Y. Wang, *J. Solid State Electrochem.* **2012**, 17, 1049.
- [191] J.-Z. Kong, C. Ren, G.-A. Tai, X. Zhang, A.-D. Li, D. Wu, H. Li, F. Zhou, *J. Power Sources* **2014**, 266, 433.
- [192] J. Zhao, Y. Wang, *J. Phys. Chem. C* **2012**, 116, 11867.
- [193] X. Li, J. Liu, X. Meng, Y. Tang, M. N. Banis, J. Yang, Y. Hu, R. Li, M. Cai, X. Sun, *J. Power Sources* **2014**, 247, 57.
- [194] M. R. Laskar, D. H. Jackson, S. Xu, R. J. Hamers, D. Morgan, T. F. Kuech, *ACS Adv. Mater. Interfaces* **2017**, 9, 11231.
- [195] J. S. Park, X. Meng, J. W. Elam, S. Hao, C. Wolverton, C. Kim, J. Cabana, *Chem. Mater.* **2014**, 26, 3128.
- [196] S. Deng, B. Xiao, B. Wang, X. Li, K. Kaliyappan, Y. Zhao, A. Lushington, R. Li, T.-K. Sham, H. Wang, X. Sun, *Nano Energy* **2017**, 38, 19.
- [197] A. Kraytsberg, H. Drezner, M. Auinat, A. Shapira, N. Solomatin, P. Axmann, M. Wohlfahrt-Mehrens, Y. Ein-Eli, *ChemNanoMat* **2015**, 1, 577.

- [198] J. S. Park, A. U. Mane, J. W. Elam, J. R. Croy, *Chem. Mater.* **2015**, *27*, 1917.
- [199] J. Xie, A. D. Sendek, E. D. Cubuk, X. Zhang, Z. Lu, Y. Gong, T. Wu, F. Shi, W. Liu, E. J. Reed, Y. Cui, *ACS Nano* **2017**, *11*, 7019.
- [200] a) B. H. Lee, B. Yoon, A. I. Abdulagatov, R. A. Hall, S. M. George, *Adv. Funct. Mater.* **2013**, *23*, 532; b) B. H. Lee, B. Yoon, V. R. Anderson, S. M. George, *J. Phys. Chem. C* **2012**, *116*, 3250; c) Y. Zhao, L. V. Goncharova, Q. Zhang, P. Kaghazchi, Q. Sun, A. Lushington, B. Wang, R. Li, X. Sun, *Nano Lett.* **2017**, *17*, 5653.
- [201] a) B. Yoon, B. H. Lee, S. M. George, *J. Phys. Chem. C* **2012**, *116*, 24784; b) S. E. Atanasov, M. D. Losego, B. Gong, E. Sachet, J. P. Maria, P. S. Williams, G. N. Parsons, *Chem. Mater.* **2014**, *26*, 3471.
- [202] A. I. Abdulagatov, K. E. Terauds, J. J. Travis, A. S. Cavanagh, R. Raj, S. M. George, *J. Phys. Chem. C* **2013**, *117*, 17442.
- [203] P. Poodt, D. C. Cameron, E. Dickey, S. M. George, V. Kuznetsov, G. N. Parsons, F. Roozeboom, G. Sundaram, A. Vermeer, *J. Vac. Sci. Technol., A* **2012**, *30*, 010802.
- [204] P. Poodt, J. van Lieshout, A. Illiberi, R. Knaapen, F. Roozeboom, A. van Asten, *J. Vac. Sci. Technol., A* **2013**, *31*, 01A108.
- [205] P. S. Maydannik, T. O. Kääriäinen, K. Lahtinen, D. C. Cameron, M. Söderlund, P. Soininen, P. Johansson, J. Kuusipalo, L. Moro, X. Zeng, *J. Vac. Sci. Technol., A* **2014**, *32*, 051603.
- [206] a) S. Adhikari, S. Selvaraj, D.-H. Kim, *Adv. Mater. Interfaces* **2018**, *5*, 1800581; b) D. Longrie, D. Deduytsche, J. Haemers, K. Driesen, C. Detavernier, *Surf. Coat. Technol.* **2012**, *213*, 183.
- [207] Y. Zhao, X. Sun, *ACS Energy Lett.* **2018**, 899.
- [208] G. Assat, J.-M. Tarascon, *Nat. Energy* **2018**, *3*, 373.
- [209] S. Chen, J. Zheng, L. Yu, X. Ren, M. H. Engelhard, C. Niu, H. Lee, W. Xu, J. Xiao, J. Liu, J.-G. Zhang, *Joule* **2018**, *2*, 1548.